Instituut voor Natuur- en Bosonderzoek - Kliniekstraat 25 - 1070 Brussel - T.: +32 (0)2 558 18 11 - F.: +32 (0)2 558 18 05 - info@inbo.be - www.inbo.be

Case Kleine Nete : hydrologie

Wetenschappelijk rapport - NARA 2009

Jef Dams, Elga Salvadore, Toon Van Daele, Okke Batelaan

INBO.R.2009.28

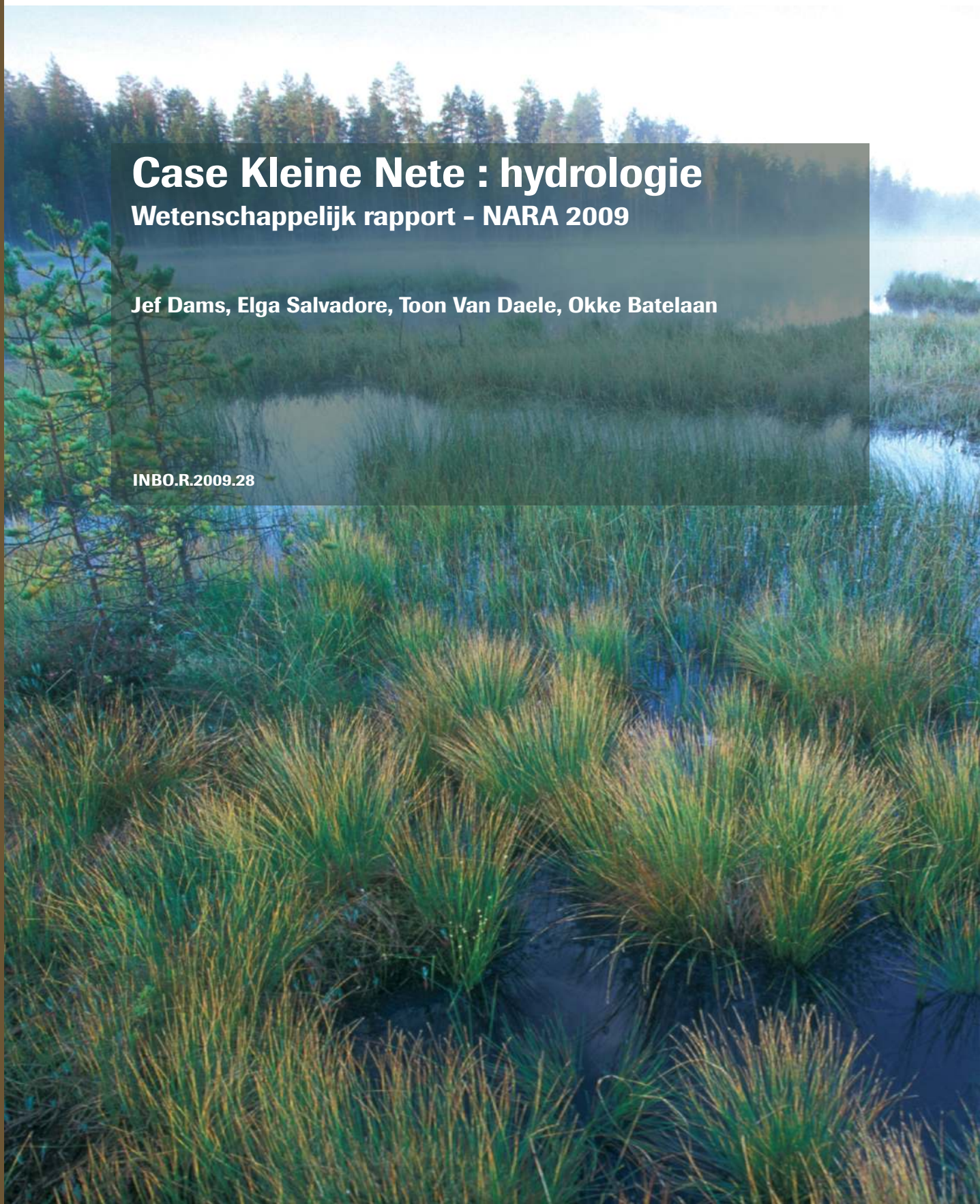

Vlaamse overheid

Auteurs:
Jef Dams, Elga Salvadore, Okke Batelaan,
Vrije Universiteit Brussel

Toon Van Daele,
Instituut voor Natuur- en Bosonderzoek

Instituut voor Natuur- en Bosonderzoek
Het Instituut voor Natuur- en Bosonderzoek (INBO) is het Vlaams onderzoeks- en kenniscentrum voor natuur en het duurzame beheer en gebruik ervan. Het INBO verricht onderzoek en levert kennis aan al wie het beleid voorbereidt, uitvoert of erin geïnteresseerd is.

Vestiging:
INBO Brussel
Kliniekstraat 25, 1070 Brussel
www.inbo.be

e-mail:
toon.vandaele@inbo.be

Wijze van citeren:
Dam J. , Salvadore E., Van Daele T. & Batelaan, O. (2009) Case Kleine Nete: hydrologie, Wetenschappelijk rapport, NARA-2009. [INBO.R.2009.28]. Rapporten van het Instituut voor Natuur- en Bosonderzoek 2009 (28). Instituut voor Natuur- en Bosonderzoek, Brussel.

D/2009/3241/492
INBO.R.2009.28
ISSN: 1782-9054

Verantwoordelijke uitgever:
Jurgen Tack

Foto cover:
Vilda Photo

Dit onderzoek werd uitgevoerd in samenwerking met:
de Vrije Universiteit Brussel

NARA 2009 - Wetenschappelijk rapport

Deelproject hydrologie

In opdracht van Instituut voor Natuur- en Bosonderzoek (INBO.FB.2008.5)

Auteurs:

Jef Dams (VUB, Dept of Hydrology and Hydraulic Engineering)
Elga Salvadore (VUB, Dept of Hydrology and Hydraulic Engineering)
Prof. Okke Batelaan (VUB, Dept of Hydrology and Hydraulic Engineering)
Toon Van Daele (INBO)

Lectoren:

Willy Huybrechts (INBO)
Els De Bie (Vlaamse Milieumaatschappij)
Wim Mertens (Agentschap voor Natuur en Bos)
Toon Van Daele (INBO)

D/2009/3241/284 INBO.R.2009.28

Content

List of figures

List of tables

1 Context

1.1 Toekomstverkenning milieu en natuur

De Milieuverkenning 2030 (MIRA 2009) en de Natuurverkenning 2030 (NARA 2009) beschrijven de toekomst van het leefmilieu en van de natuur in Vlaanderen. Het doel is de beleidsmakers en het geïnteresseerde publiek inzicht te geven in te verwachten evoluties van het leefmilieu en van de natuur in Vlaanderen, bij bepaalde beleidskeuzes en binnen een gegeven sociaal-economische context.

Dit wetenschappelijk rapport maakt deel uit van een reeks rapporten die de wetenschappelijke onderbouwing van MIRA 2009 en NARA 2009 bevatten.

1.2 Scenario's

De Natuurverkenning 2030 beschrijft de mogelijke evolutie van de natuur in Vlaanderen tijdens de periode 2005–2030 aan de hand van drie landgebruikscenario's:

- In het scenario referentie (*R) wordt het beleid uit de periode 2000-2007 ongewijzigd voortgezet en worden de voorziene plannen uitgevoerd.
- Het scenario scheiden (*S) verdeelt de open ruimte tussen de gebruiksvormen ervan, en groepeert die gebruiksvormen ruimtelijk in homogene clusters (terrestrische verkenning). Ontsnippering van waterlopen gebeurt prioritair in functie van soorten van Europees belang (aquatische verkenning).
- In het scenario verweven (*V) maakt de zorg voor natuur integraal deel uit van alle landgebruiksvormen, en worden de gebruiksvormen van de open ruimte ruimtelijk door elkaar verweven (terrestrische verkenning). Ontsnippering van waterlopen richt zich op de grotere verbindingen in het waterlopennetwerk (aquatische verkenning).

Elk landgebruikscenario bestaat uit een pakket beleidsmaatregelen waarvan het gezamenlijk effect wordt berekend. Bij de samenstelling van de pakketten wordt gestreefd naar een vergelijkbare kostprijs per scenario. Langetermijndoelstellingen van het natuur-, bos- en waterbeleid vormen een toetsingskader om de verwachte effecten te beoordelen.

De drie landgebruikscenario's in de Natuurverkenning 2030 zijn elk geënt op twee milieuscenario's uit de Milieuverkenning 2030:

- In het scenario referentie (R*) wordt het beleid uit de periode 2000-2007 ongewijzigd voortgezet en worden de voorziene plannen uitgevoerd.
- In het scenario Europa (E*) worden bijkomende inspanningen genomen om tegen 2020-2030 de Europese milieudoelstellingen te halen. De aquatische verkenning bevat twee varianten van het Europascenario, aansluitend op de scenario's in de ontwerp stroomgebiedbeheerplannen. In het scenario Europa 2027 (E27*) wordt een maximale set van aanvullende maatregelen uitgevoerd om tegen 2027 de Europese doelstelling te halen. In het scenario Europa 2015 (E15*) worden enkel tegen 2015 de meest haalbare aanvullende maatregelen uitgevoerd.

De landgebruiks- en de milieuscenario's worden uitgetekend binnen éénzelfde sociaal-economische verkenning. In de terrestrische verkenning worden ook klimaatverkenningen verwerkt, afgeleid uit internationale klimaatscenario's.

Het voornaamste zichtjaar is 2030. Voor het klimaat worden ook 2050 en 2100 als zichtjaren gehanteerd. De aquatische scenario's focussen op 2015 en 2027, aansluitend op de Europese Kaderrichtlijn water.

Voor de zes terrestrische scenario's (figuur 1) en de negen aquatische scenario's (figuur 2) worden de verwachte ontwikkelingen doorgerekend door middel van rekenkundige modellen.

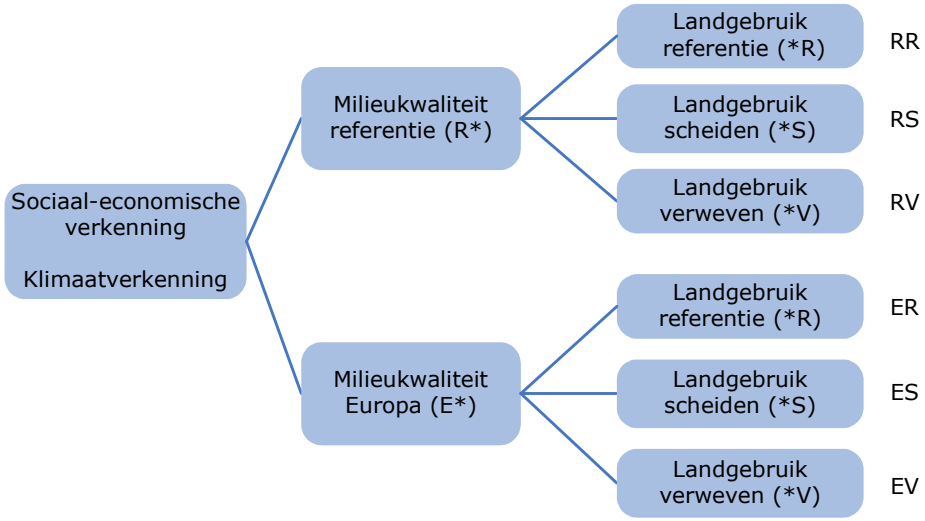

Figuur 1: Een sociaal-economische verkenning, twee milieuscenario's (gekoppeld aan twee klimaatverkenningen) en drie landgebruikscenario's worden gecombineerd in zes scenario's.

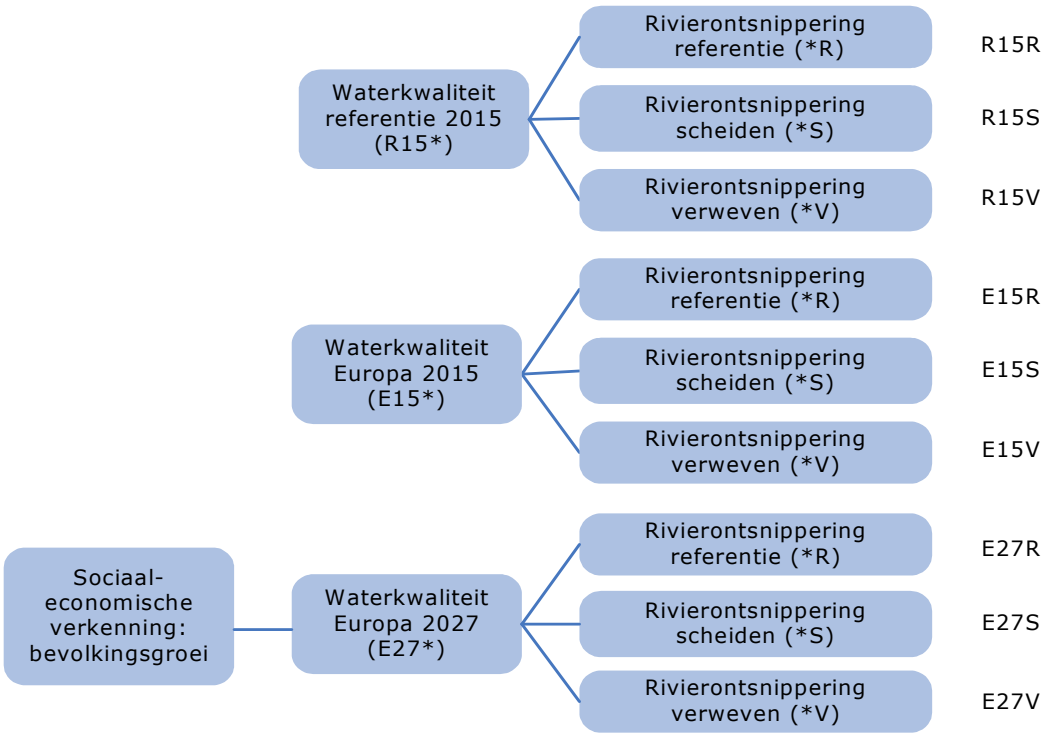

Figuur 2: Een sociaal-economische verkenning, drie milieuscenario's en drie rivierontsnipperingsscenario's worden gecombineerd tot negen scenario's.

De berekeningen gebeuren in de meeste gevallen gebiedsdekkend op niveau Vlaanderen, tenzij de beschikbare gegevens en/of modellen dit niet toelaten.

1.3 Scenarioberekeningen en onderlinge samenhang

De scenario's werden met gepaste rekenkundige modellen doorgerekend volgens het stroomschema in figuur 3.

De sociaal-economische verkenning en de klimaatverkenningen vormen een onafhankelijke input.

1. Willems P., Deckers P., De Maeyer Ph., De Sutter R., Vanneuville W., Brouwers J., Peeters B. (2009) Klimaatverandering en waterhuishouding. Wetenschappelijk rapport, MIRA 2009, NARA 2009, VMM, INBO.R.2009.49, www.milieurapport.be, www.nara.be
2. Demarée G., Baguis P., Debontridder L., Deckmyn A., Pinnock S., Roulin E., Willems P., Ntegeka V., Kattenberg A., Bakker A., Bessembinder J., Lenderink G., Beersma J. (2009) Eindverslag studieopdracht "Berekening van klimaatscenario's voor Vlaanderen" uitgevoerd door KMI, KNMI, KUL. Instituut voor Natuur- en Bosonderzoek (INBO), Brussel, INBO.R.2009.48, www.nara.be

De milieuscenario's leiden tot verkenningen inzake zowel atmosferische deposities als waterkwaliteit.

3. Schneiders A., Simoens I., Belpaire C. (2009) Waterkwaliteitscriteria opstellen voor vissen in Vlaanderen. Wetenschappelijk rapport, NARA 2009. INBO.R.2009.22, www.nara.be
4. Wuyts K., Staelens J. De Schrijver, A., Verheyen K. Overloop S., Vancraeynest L., Hens M. & Wils C. (2009) Overschrijding kritische lasten. Wetenschappelijk rapport, mira 2009, nara 2009, VMM, INBO.R.2009.55, www.milieurapport.be, www.nara.be

De landgebruikscenario's en de milieuscenario's leiden tot verkenningen inzake landgebruik. De gelijkschakeling van de kosten komt aan bod in een afzonderlijk rapport.

5. Van Reeth, W. (2009) Kosten en beleidsprestaties. Wetenschappelijk rapport, NARA 2009. INBO.R.2009.19, www.nara.be.
6. Hens M., Van Reeth W. & Dumortier M. (2009) Scenario's. Wetenschappelijk rapport, NARA 2009. INBO.R.2009.18, www.nara.be.
7. Gobin A., Uljee I., Van Esch L., Engelen G., de Kok J., van der Kwast H., Hens M., Van Daele T., Peymen J., Van Reeth W., Overloop S., Maes F. (2009) Landgebruik in Vlaanderen. Wetenschappelijk rapport, MIRA 2009, NARA 2009, VMM, INBO.R.2009.20, www.milieurapport.be, www.nara.be.
8. Overloop S., Gavilan J., Carels K., Van Gijseghem D., Hens M., Bossuyt M., Helming J. (2009) Landbouw. Wetenschappelijk rapport, MIRA 2009 & NARA 2009, VMM, INBO.R.2009.30, www.milieurapport.be, www.nara.be.

De verkenningen inzake landgebruik worden doorgerekend naar verkenningen inzake biotopen en habitats. Deze worden met de verkenningen inzake atmosferische deposities geconfronteerd, hetgeen resulteert in verkeningen inzake de druk van atmosferische vermestende en verzurende deposities op biotopen.

9. Van Daele T. (2009) Biotopen. Wetenschappelijk rapport, NARA 2009. INBO.R.2009.23, www.nara.be.

In een gevalstudie voor de Kleine Nete worden de verkenningen inzake landgebruik ook geconfronteerd met de klimaatverkenningen om via hydrologische modellering tot een verfijnde verkenning van de habitats te komen.

10. Dam J. , Salvadore E., Van Daele T. & Batelaan, O. (2009) Case Kleine Nete: hydrologie. Wetenschappelijk rapport, NARA 2009. INBO.R.2009.28, www.nara.be.

11. Van Daele T. (2009) Case Kleine Nete: moerasvegetaties. Wetenschappelijk rapport, NARA 2009. INBO.R.2009.25, www.nara.be.

De verkenningen inzake biotopen en habitats en de klimaatverkenningen vormen de input voor verkenningen inzake terrestrische soorten.

12. De Bruyn L. & Bauwens D. (2009) Terrestrische soorten. Wetenschappelijk rapport, NARA 2009. INBO.R.2009.26, www.nara.be.

Aan de landgebruikscenario's worden ook scenario's inzake rivierontsnippering gekoppeld. Zij worden vertaald naar verkenningen inzake rivierontsnippering. Samen met de scenario's inzake waterkwaliteit en een typering van het rivierennetwerk, vormen zij de basis voor verkenningen inzake aquatische soorten.

13. Schneiders A., Van Daele T. & Wils C. (2009) Huetzonering van het rivierennetwerk in Vlaanderen. Wetenschappelijk rapport, NARA 2009. INBO.R.2009.24, www.nara.be.
14. Stevens M. & Schneiders A. (2009) Scenario's voor het oplossen van migratieknelpunten voor vissen. Wetenschappelijk rapport, NARA 2009. INBO.R.2009.21, www.nara.be.
15. Schneiders A. (2009) Vismodellering. Wetenschappelijk rapport, NARA 2009. INBO.R.2009.27, www.nara.be.

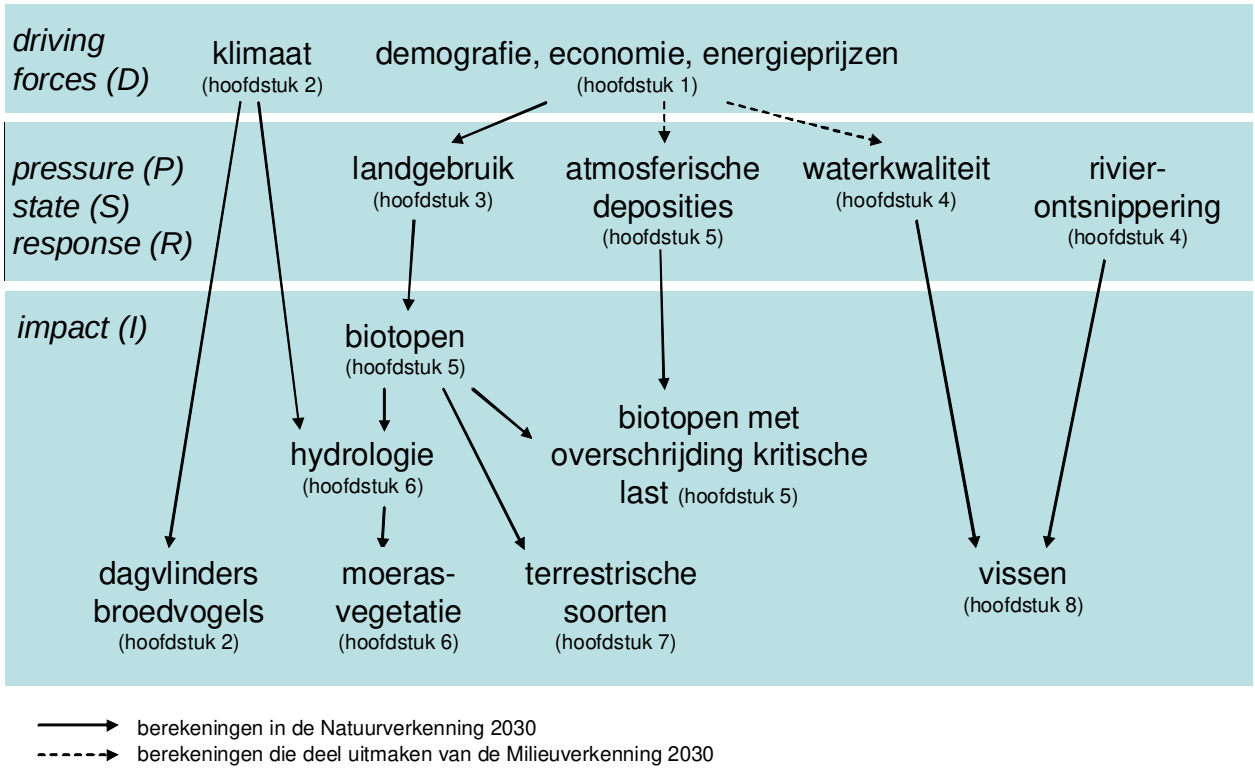

Figuur 3: Stroomschema en samenhang van de scenarioberekeningen.

2 Introduction

2.1 General Introduction

Global anthropogenic changes are increasingly influencing the earth's water resources, thereby threatening important ecosystems and human living conditions. Both land-cover/use and climate changes are expected to significantly influence both surface and subsurface hydrology in the near future. To plan mitigating or adaptive actions, there is a strong need to study the individual as well as the combined impact of climate and land-use changes on the river, groundwater and wetland system on both regional and local scale.

Since the origin of the earth the climate has been highly variable, driven for example by magma activity, rotation of the earth, sun activity, etc. However, current climate changes have been proven to be the first anthropogenic driven climatic changes, primarily attributed to burning of fossil fuels. As the climate is one of the controlling factors of the hydrological cycle, every change in climate can have a large impact on the global, regional or local hydrology. Climatic changes altering temperature, precipitation and other climatic variables impact the flooding threat, global soil moisture, sea level, groundwater availability and so on. Due to the major importance of water for life on earth, there is an increasing concern for future climate changes and their impacts on water resources.

Besides climate changes also land-cover changes can have a significant effect on the hydrology. Throughout the entire history of mankind, intense human utilization of land resources has resulted in significant changes of the land-use and land-cover. Since the era of industrialization and rapid population growth, land-use change phenomena have strongly accelerated in many regions.

In this study we will focus on the impact of these global changes on the groundwater system. Globally groundwater is the largest source of freshwater and plays a leading role in supplying water for human consumption, maintaining river flows and as a source of water for plants. The main challenge scientists and policy makers face concerning groundwater management is to maintain the balance between competing elements as preserving ecological importance and the use of groundwater resources for drinking water supply, industry, etc.

Because it is practically not convenient to simulate the groundwater system for the whole of Flanders on a fine spatial and temporal resolution, it is chosen to develop a case study covering only the Kleine Nete basin. Due to the sandy soils and low slopes a large fraction of the effective rainfall in the basin is percolating to the groundwater. The groundwater in the basin is extensively used for drinking water production, while important groundwater dependent wetlands are present. In the past decades strong urbanization processes have significantly changed land-use and are expected to continue, posing negative impacts on groundwater resources.

Traditionally, groundwater evaluation relied on average water balance calculations for basin-scale estimates of inflow and outflow. Though, analytical techniques were used to simulate groundwater flow and transport in aquifers with simple initial and boundary conditions, such methods cannot be used in case of heterogeneous aquifer parameters and irregular boundary conditions both in time and space. For this reason 3-dimensional groundwater flow models are required to simulate catchments with complex terrain and variable stresses. The results can be useful to assess the water resources potential of the catchment in consideration and to lay the foundation for future impact assessment.

2.2 Methodology

An overview of the methodology applied in this study is illustrated in Fig. 3. The hydrological part is shown in the blue box. Main variable inputs for this study are the forecasted climate and land-use scenarios. Two models are used to study the impact of the changing land-use and climate on the groundwater system:

- WetSpa model simulates the groundwater recharge and the river discharge under the different scenario conditions
- MODFLOW model simulates the groundwater flow system of the study basin.

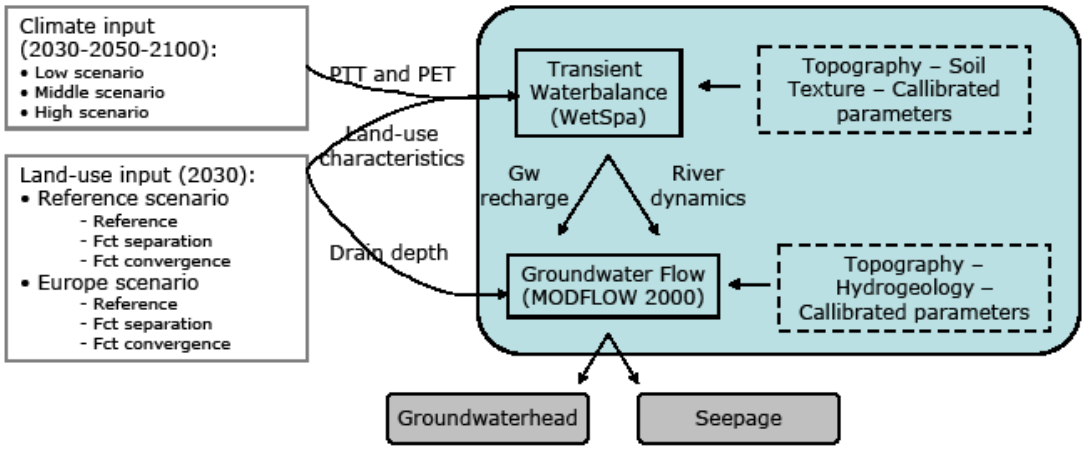

Figure 1: General overview of the applied methodology (PPT = precipitation, PET = Potential evapotranspiration)

The WetSpa model requires climatic input such as precipitation and potential evapotranspiration, land-use, topography and soil texture. When the hydrological model is build for a specific basin the model needs to be calibrated.

Building the MODFLOW groundwater flow model requires next to a substantial amount of geo-hydrological data the groundwater recharge, river head and drain level: the groundwater recharge is taken from the WetSpa model, river heads from interpolated stage data and the drain level is read from soil classifications and is adapted according to the land-use change.

The models are calibrated for the period 1992-2001, this period was chosen due to the availability of river discharge data and groundwater head data required for the calibration of respectively the WetSpa and MODFLOW model. The period from 1960 until 1991 (32 years) is chosen to represent the current climate condition. An overview of the time periods for the current, future and calibrated models is given in Figure 4.

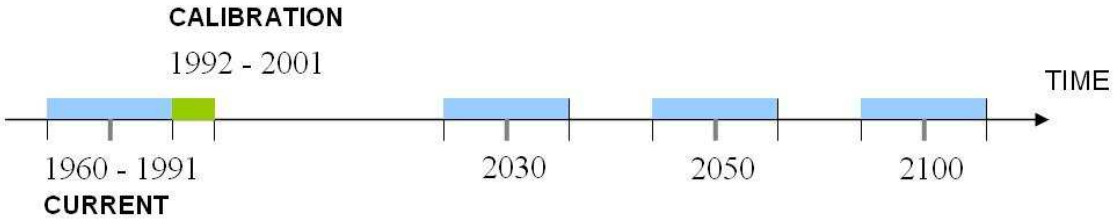

Figure 2: Timescale indicating periods for current model, calibrated model and future scenarios

The model timestep was chosen one day and half a month for the WetSpa and MODFLOW model respectively. The half monthly recharge is aggregated from daily recharge output obtained from WetSpa.

2.3 Investigated scenarios

Table 1 gives an overview of the scenarios that have been investigated for their hydrological impact. The blocks in green are scenarios, which are simulated in both WetSpa and MODFLOW and are analysed for their impacts on the hydrological conditions. The current land-use (2005) with the current climate condition is chosen as the reference scenario.

Tabel 1: overview scenarios

		Climate									
		Current	2030			2050			2100		
			Low	Mid	High	Low	Mid	High	Low	Mid	High
Land-use											
Current (2005)	RR05										
Reference scenario											
Referentie - Referentie	RR30										
Referentie - Scheiden	RS30										
Referentie - Verweven	RV30										
Europe scenario											
Europa - Referentie	ER30										
Europa - Scheiden	ES30										
Europa - Verweven	EV30										

3 Study area Kleine Nete

The study area is located in Belgium about 60 km north-east of Brussels (Fig. 5). It comprises 581 km² and covers a major part of the Kleine Nete basin. The study basin is part of the Nete basin, comprising the Kleine Nete and the Grote Nete basin, and has a total area of 1673 km². The Nete basin on its turn is a part of the Scheldt basin, draining 21860 km² towards the North Sea. The river discharge station situated in Grobbendonk, managed by the Hydrologic Information Centre (HIC), is chosen as the outlet of our study basin.

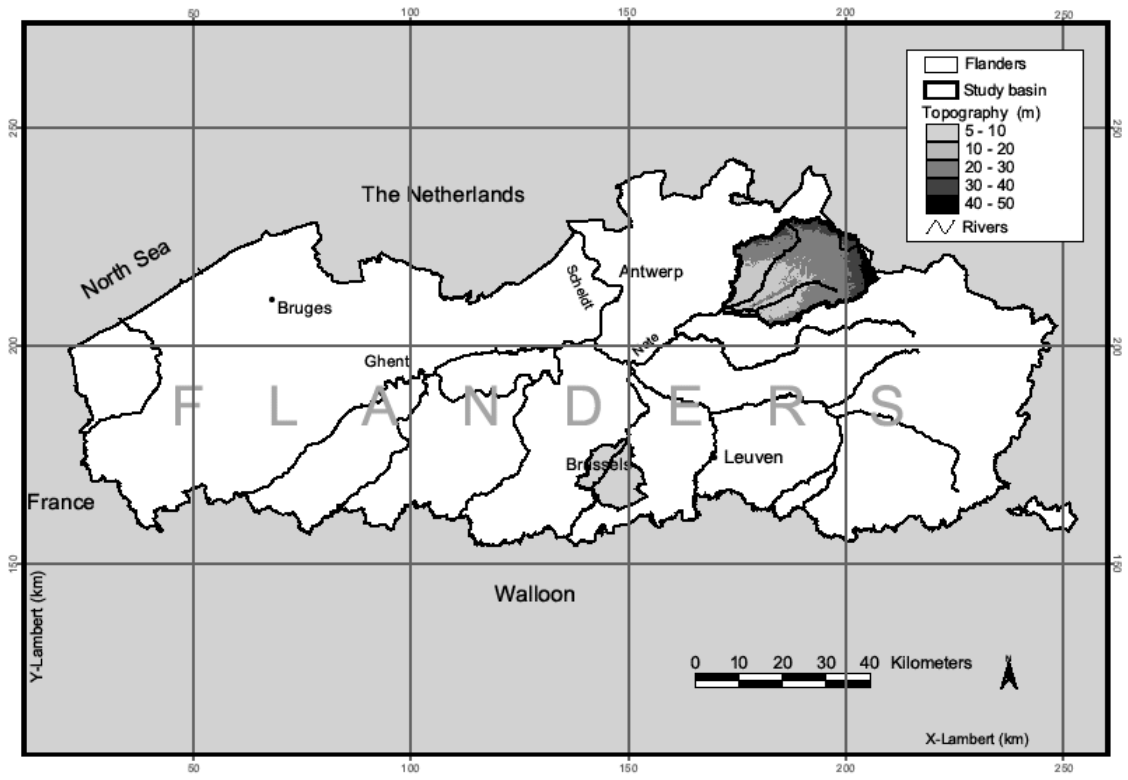

Figure 3: Location of the study area

The average precipitation in the area is about 840 mm/y. The dominant soil texture is sand, though in the valleys some loamy sand, sandy loam and sandy clay is present.

3.1 Topography

The Kleine Nete basin is characterized by a moderate rolling landscape cut by the Kleine Nete River, the Aa River and their tributaries, resulting in long stretched hills, very slightly elevated interfluves and broad swampy valleys (Wouters and Vandenberghe, 1994). Figure 6 shows the topographic elevation of the catchment. It was resampled to 50 m resolution from the original 25 m resolution digital elevation model of Flanders (0C GIS-Vlaanderen 2001). The basin is relatively flat with the topography ranging from 3 to 48m, with an average of 24 m above sea level, while the means slope is 0.36%. There is a gradual decrease of the elevation from the Campine plateau, situated on the eastern side of the basin and shown in blue on Fig. 6. The highest slopes are found between the Kleine Nete and the Aa Rivers on the Campine ridge (Dutch: Kempense heuvelrug) (Baten and Huybrechts, 2002).

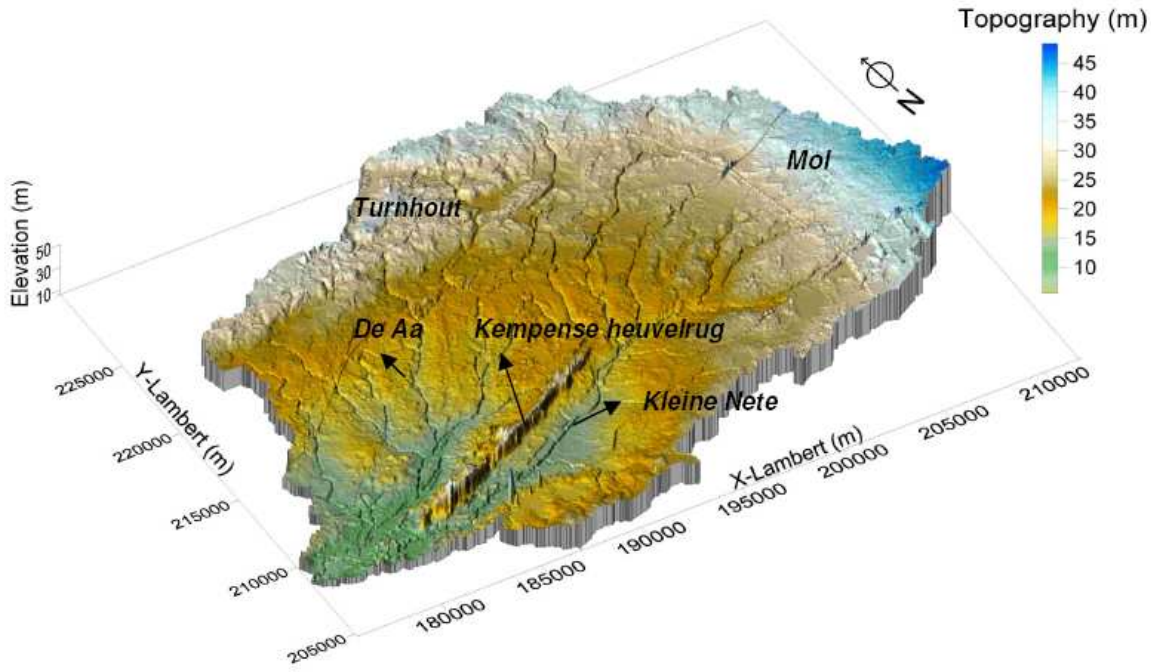

Figure 4: Topography of the Kleine Nete Catchment.

3.2 Geology

Geologically the study area belongs to the Campine basin, a subsidence area north of the Massive of Brabant (Wouters and Vandenberghe, 1994). Geologic formations from the Cenozoic Era constitute the aquifer systems of the Kleine Nete catchment. During the Oligocene epoch (last epoch of the Paleogene period), the 'Boom Clay' was deposited in the basin. This clay layer is extensively studied for its potential to store high-level and long-lived radioactive waste (Wemaere et al., 2008). Wemaere et al. (2008) estimated the vertical hydrological conductivity of the Boom Clay as approximately 2.8 10^{-12} m/sec. This low vertical conductivity means that the Boom Clay layer can be considered to be an impervious base of the aquifer system. Table 2 gives an overview of the different aquifers. Figure 7 – 10 give some cross-sections of the hydrogeology.

The regional geological composition of the aquifer system of the Nete catchment can be schematized as a four-layer system with the top of the Formation of Boom as its bottom boundary. The stratigraphy of the geological layers of the area is as follows (Wouters and Vandenberge, 1994):

i. The Formations of Diest and Berchem were deposited in a marine environment during the Miocene. The Formation of Berchem contains glauconitic and clay rich fine sands with mica and shells. The Formation of Diest consists of green-grey coarse glauconite containing sandy soils. The overall groundwater flow direction in the 75 m thick aquifer of the Formations of Diest and Berchem is SE-NW. The aquifer system has a transmissivity of 1200 m²/day, estimated from pumping test results (Woldeamlak, 2007).
ii. The Formations of Lillo, Kattendijk and Kasterlee are sand deposits from the Pliocene when the study area was dominated by a shallow marine environment. The Formation of Kasterlee, which is in our study area more abundant then the Lillo and Kattendijk Formations, forms a discontinuous layer covering the sandy Formation of Diest and Berchem. At its base, the Formation of Kasterlee is clayey, dividing the aquifer system in a semi-confined aquifer of the Formations of Diest and Berchem, and a phreatic aquifer of the Formation of Kasterlee and quaternary (loamy) sands.
iii. The Formation of Mol, Brasschaat and Merksplas were deposited during the end of the Pliocene and the Pleistocene epoch (Quaternary period) by the River Rhine, at that time flowing from southeast to northwest.
iv. Quaternary sandy or loamy-sandy sediments. The Campine Complex was formed in the northern part of the Nete catchment (Beerse, Rijkevorsel and Turnhout). The complex of the Campine has a thickness of about 25 m and consist of fine sands with clay layers. During the late Pleistocene, the study area was covered by an eolian sand and loess layer of about two meters thick. Finally, during the Holocene, the existing river valley was filled with fluvial sediments with an average thickness of one meter.

Tabel 2: Overview of aquifers and their parameters based on the HCOV classification for Flanders (Woldeamlak, 2007).

Aquifer code (HCOV)	Aquifer name	Total hydraulic conductivity (m/d)		Storage coefficient (-)
		Average	Range	
0100	The Quaternary aquifer systems	4.8	1-10	$2.7 * 10^{-5} – 2.6 *10^{-1}$
0220	The clay-sand-complex of the Kempen	9.4	5-15	$7.9 * 10^{-4} – 1.5 *10^{-3}$
0230	The Pleistocene and Pliocene aquifer	20.5	4-40	$2.5 * 10^{-5} – 3.7 *10^{-3}$
0240	The Pliocene clayey layer	0.1	0.04 -0.2	$1.2 * 10^{-5}$
0250	The Miocene aquifer system	14.1	3-30	$1.3 * 10^{-5} – 4.1 *10^{-2}$

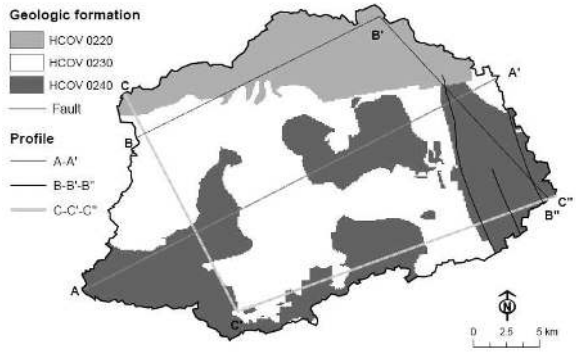

Figure 5: Occurrence of the tertiary aquifers: HCOV 0220, 0230, 0240 and geologic faults.

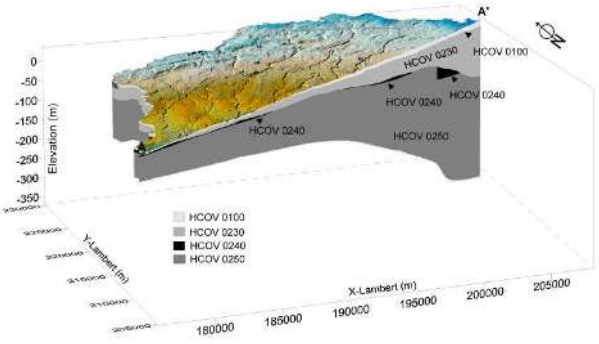

Figure 6: cross-section along profile A-A' showing the different tertiary aquifers.

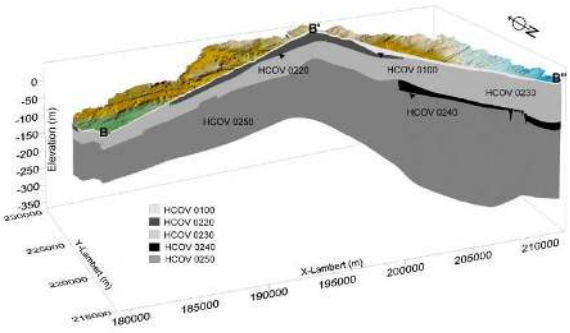

Figure 7: cross-section along profile B-B'-B'' showing the different tertiary aquifers.

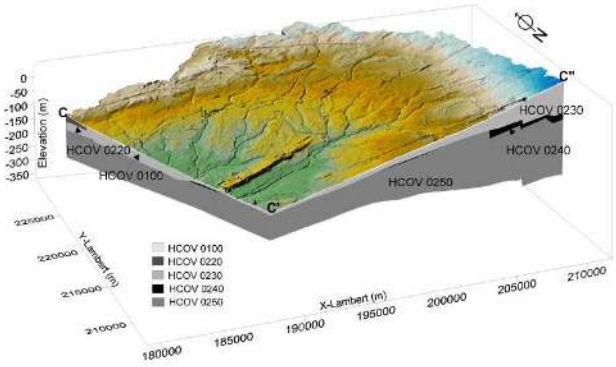

Figure 8: cross-section along profile C-C'-C'' showing the different tertiary aquifers.

3.3 Land-use

Figure 11 shows the present land-use in the Kleine Nete basin. The map is created by Toon Van Daele (INBO, 2008) based on different GIS resources. The largest urban centre in the basin is Turnhout with about 40.000 inhabitants. A number of small urban centres are situated in the basin, e.g. Beerse, Arendonk, Retie, Kasterlee, Lichtaart, Tielen, Gierle, Lille, Vosselaar and Vorselaar. The population in these smaller centres ranges roughly from 1000-10.000 people.

Forest is most abundant on the Campine ridge (see Fig. 6) and at the northern and eastern parts of the basin. The most common forest type is evergreen needle. In the south-east of the basin there are some lakes. These lakes are the result of the excavation of the sands of Mol, which are among other used for the production of glass.

Agriculture is very important in the basin, especially with regard to the land-use. Most farms are dairy or livestock farms resulting in a large area of agricultural grassland and a high mais production.

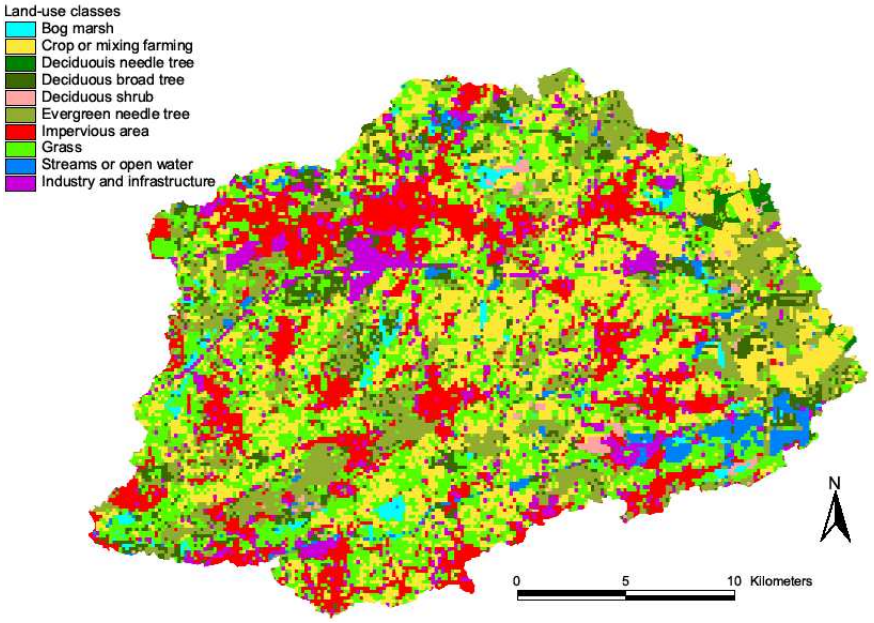

Figure 9: Land-use map 2005

In 2005, the land-use of the study area consisted of 26% grassland (including grassland-used for agriculture, parks, etc.), 23% crop or mixed farming, 17% urban area, 14% coniferous forest, 8% deciduous forest, 6% industrial and infrastructure area, 3% open water, 2% bog marsh, 1% heather. The land-use classes used in Fig. 11 and 12 are the ones used by the WetSpa model described later in this report.

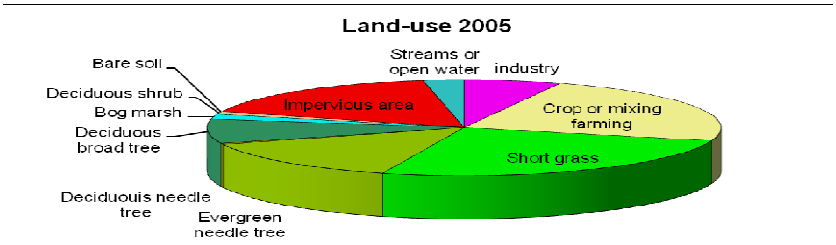

Figure 10: Area covered by each land-use type

3.4 Current climate

A detailed description of the climate in Belgium is given by Demarée et al. (2009), a more specific description for the Nete basin is given in part 2 of the basin management plan of the Nete basin (Soresma, 2002). A short description of the most important meteorological characteristics of the basin is given below.

The region has a temperate climate characterized by a warm summer and a cool winter with little snowfall. The long term temperature data shows a uni-modal distribution, with long term average winter and summer temperatures of 5 and 14°C respectively. The long term mean annual precipitation ranges from about 600 to 1100 mm with an areal average of 828 mm, almost equally distributed over the winter and summer periods. In this study winter months refer to October till March, while summer months are April to September. The long term average annual potential evapotranspiration is about 670 mm.

The meteorological data of rainfall, potential evaporation and temperature used throughout the study are obtained from the Royal Meteorological Institute of Belgium (KMI).

3.4.1 Rainfall

In hydrological modelling the rainfall input is of major importance to estimate hydrological fluxes as good as possible. In the case of distributed hydrological models, such as the WetSpa model, the modeller should include as much as possible the spatial distribution of the rainfall. Therefore it is important to include as much rainfall gauges as possible. In this project five rainfall gauges were incorporated: Rijkevorsel, Turnhout, Klein Brogel, Geel and Viersel. The Thiessen polygon approach is used to search for the rainfall station closest to every raster cell. The result is shown in Fig. 13.

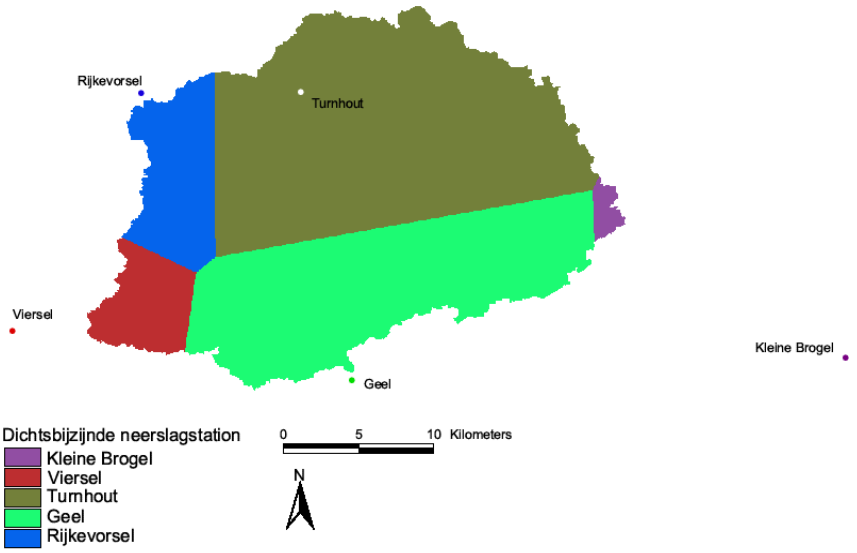

Figure 11: Rainfall distribution

In this study we will use the period 1960 until 1991 as the reference period for the current climate. Fig. 14 illustrates the annual precipitation amounts during this reference period with respect to the average annual precipitation during 32 years: 828.4 mm. The blue lines visible on the same figure indicate the standard deviation.

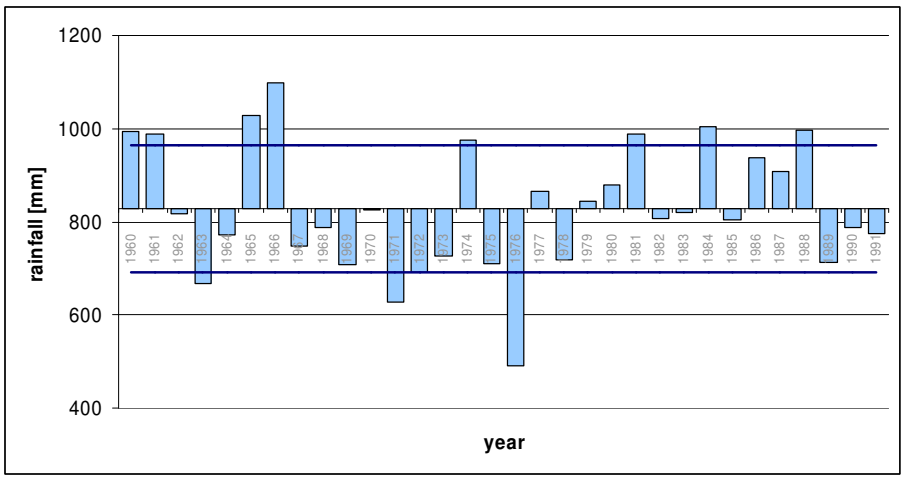

Figure 12: Annual precipitation during reference period (1960 - 1991)

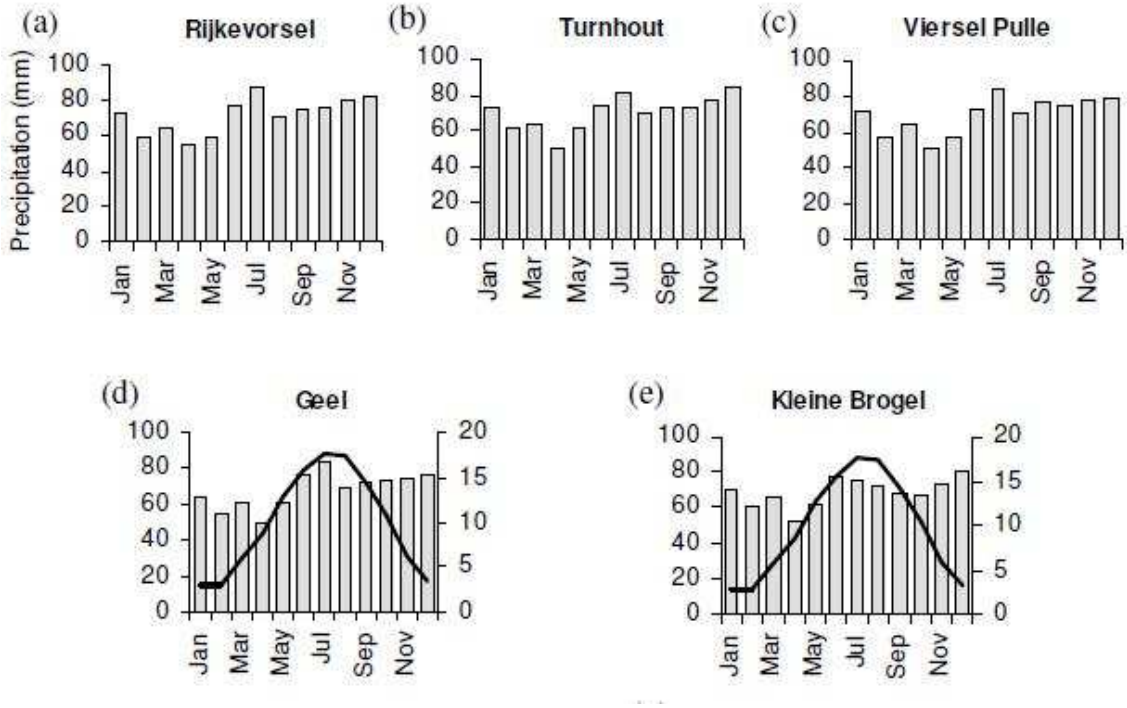

Figure 13: Average monthly precipitation at rainfall gauges Rijkevorsel (a), Turnhout (b), Viersel Pulle (c), Geel (d) and Kleine Brogel (e). The black line in figures (d) and (e) indicates the evolution in average monthly temperature over the year.

Figure 15 shows that in all rainfall stations slightly less precipitation is measured during the period February–May. The months June, July and December often have the highest precipitation. Nevertheless, monthly differences are relatively small.

3.4.2 Potential evapotranspiration

The mean monthly potential evapotranspiration (PET) for the stations of Mol (South-East of the basin) and Ukkel (near Brussels) is shown in Fig. 16. The PET is maximum during summer (June – July) and minimum during winter (December – January). The difference between the station of Mol and Ukkel is very small, even at a daily scale.

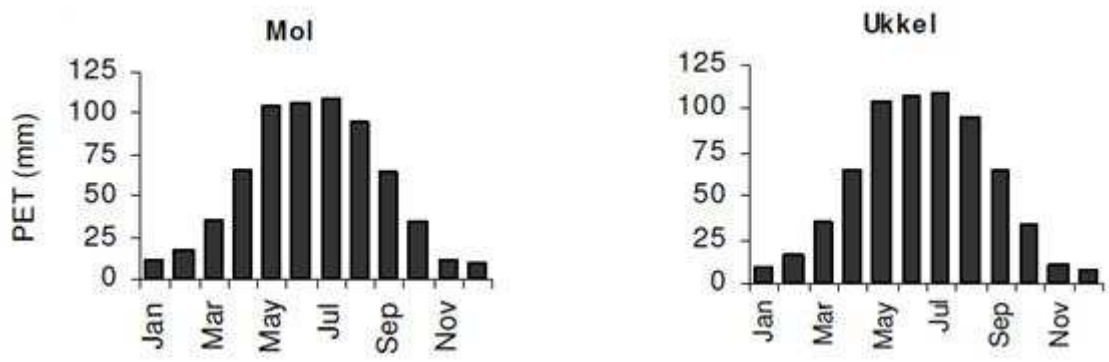

Figure 14: Mean monthly potential evapotranspiration for the meteorological station of Mol and Ukkel.

The average yearly PET during the period 1960-1991 is 664 mm. The yearly variety in PET is illustrated in Fig. 17, the blue lines again show the standard deviation interval (±47 mm).

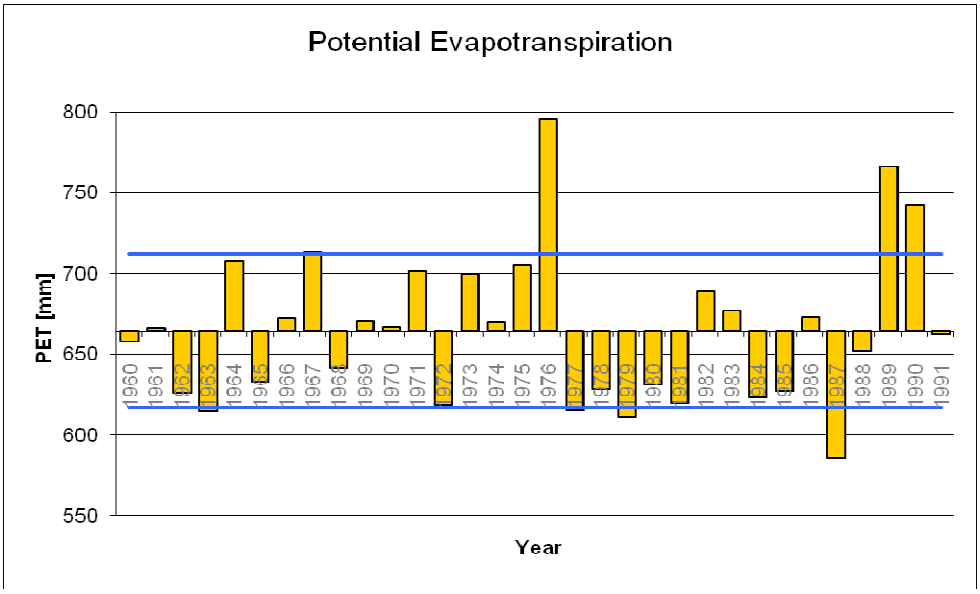

Figure 15: Yearly potential evapotranspiration (1960-1991)

3.5 Hydrology

3.5.1 Groundwater measurements

Figure 18 indicates the location of the piezometers used for the calibration of the MODFLOW model. In total 113 different piezometers or observation wells are used, spread over the entire basin. The observation wells are obtained from databases maintained by VMM and INBO. Most of the wells are read about every two weeks. In total 10226 head observations measured during the calibration period (1992-2001) are used.

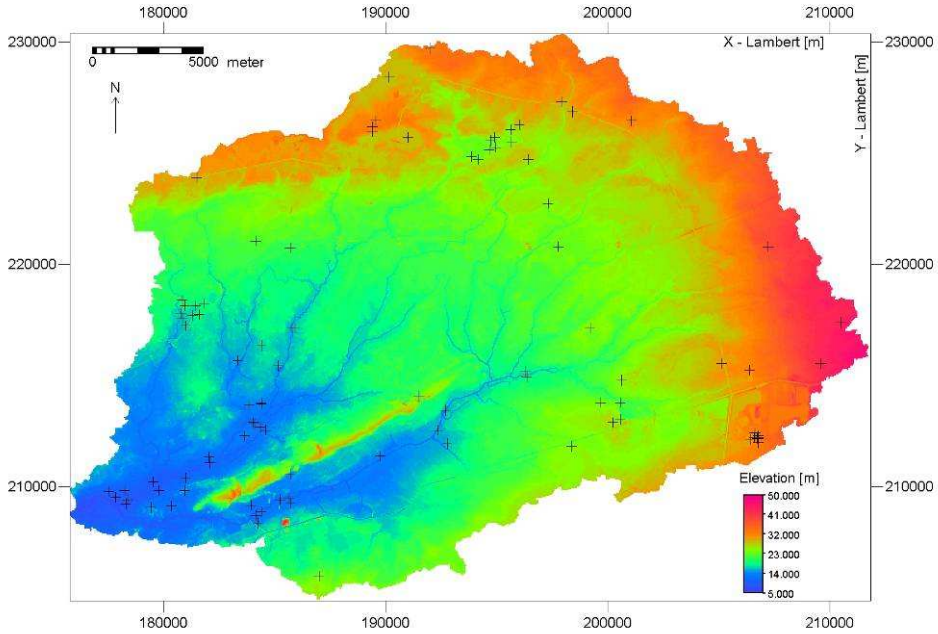

Figure 16: Piezometer locations

The GXG's (abbreviated from the Dutch gemiddelde hoogste/laagste/voorjaars grondwaterstand; average highest, lowest and spring groundwater level) are an important measure of the dynamic groundwater characteristics. The results of this hydrological study will be applied to investigate the impacts on the ecohydrology of the basin. Since, groundwater dependent vegetation is influenced primarily by the yearly lowest and highest groundwater heads, the calculation of the GXG under the different future scenarios is one of the prime goals of this study.

Three different GXG are measured and calculated:

- GHG (gemiddeld hoogste grondwaterstand / average highest groundwater level) is calculated as the average of the three highest groundwater levels (measured or simulated around every two weeks) per hydrological year (1 April – 31 March) again averaged over at least eight consecutive years.

- GLG (gemiddeld laagste grondwaterstand / average lowest groundwater level) is calculated as the average of the three lowest groundwater levels (measured or simulated around every two weeks) per hydrological year (1 April – 31 March) again averaged over at least eight consecutive years.

- GVG (gemiddelde voorjaars grondwaterstand / average spring groundwater level) is calculated as the average groundwater level of the 14th of March, the 28th of March and the 14th of April and again averaged over at least eight consecutive years. In our simulations the GVG is calculated as the average of the groundwater head during the stress period 15 March – 31 March and 1 April – 15 April, averaged for 31 years (1 April 1960 – 31 March 1991).

In general GXG's are expressed as groundwater depths below the land surface. Figure 19 shows a graph with the GXG's for a selection of the observation wells. The average GHG, GLG and GVG for these wells is respectively 0.52 m, 1.07 m and 0.62 m. The standard deviation for the three GXG is around 60 cm. Most of the observation wells included in Fig. 19 are however situated in nature reserves, many

even in groundwater dependent areas. Therefore, these values cannot be considered as representative for the entire catchment.

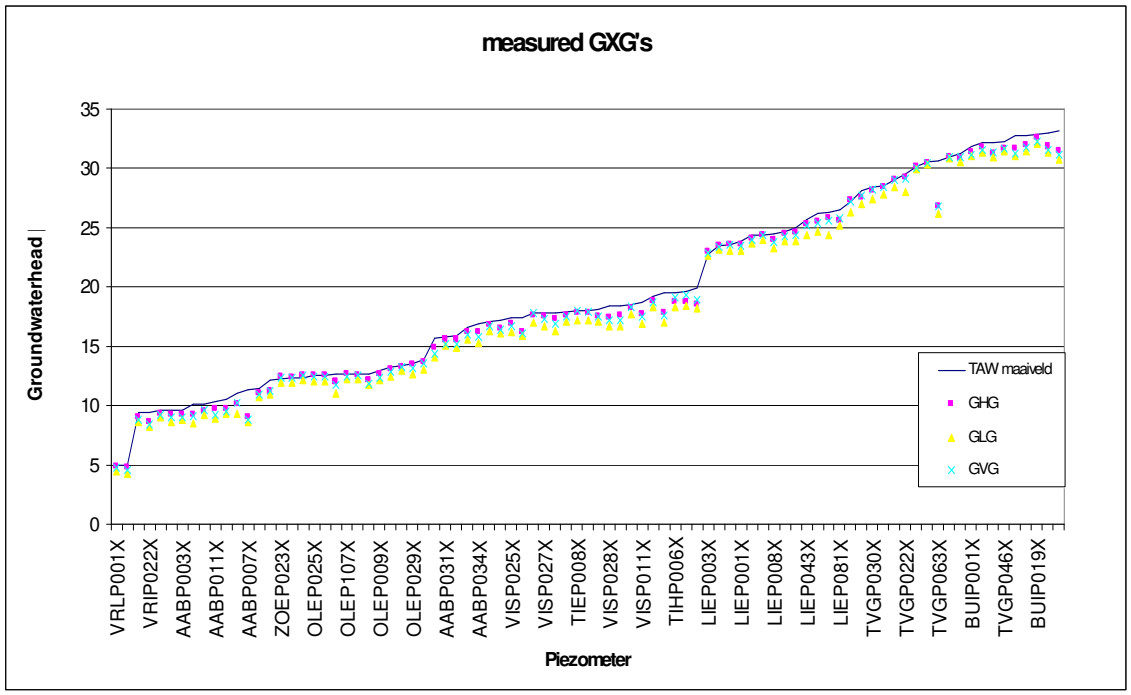

Figure 17: Observed GXG's and their position below the topography.

3.5.2 Pumping wells

A distinction is made between the permitted pumping rate, the actual pumping rate and the estimated pumping rate. If known, the actual pumping rate is used in the groundwater model; otherwise, the estimated pumping rate is used, which is expressed as percentage of the permitted pumping rate (Table 3). In total there are 565 wells, which extract a total of 54,291 m³/day. Figure 20 shows the pumping wells incorporated in the groundwater flow model. In general most of these well extractions are relatively small (< 50 m³/ d). The three largest wells pump respectively 11,310, 11,230 and 7,660 m³/day, and are used for drinking water extraction by PIDPA. Two of these wells are situated in the South of the basin and one central in the basin.

Tabel 3: Permitted versus actual pumping rates based on registered wells in Flanders for the year 2000.

Permitted rate (m³/y)	> 500000	500000 – 30000	30000 – 3560	< 3560
average actual pumping rate (%)	51.87	64.36	58.32	93.17

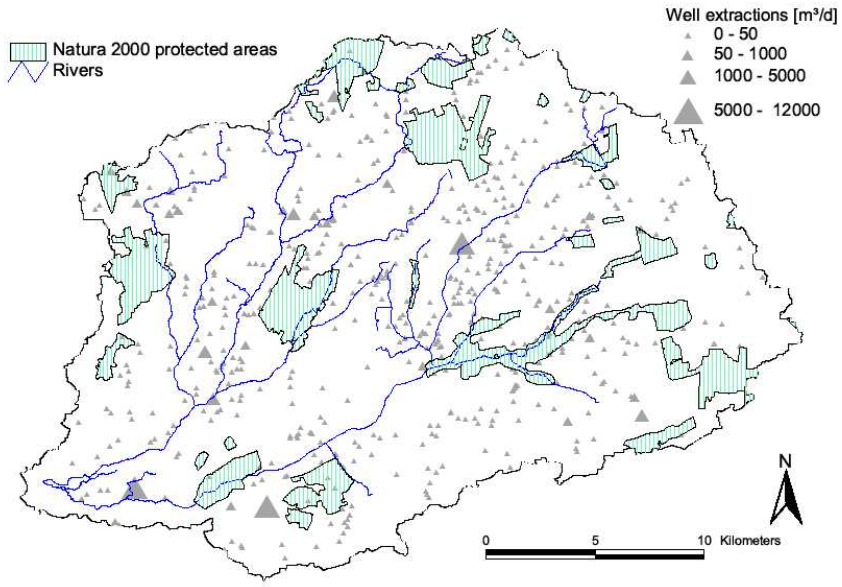

Figure 18: Well extractions and Natura 2000 areas.

3.5.3 Surface Water

Figure 21 shows the main rivers, canals and lakes in the Kleine Nete basin. Next to natural rivers and lakes two man-made canals flow through the basin: canal Dessel – Turnhout – Schoten and canal Herentals – Bocholt. The canal Dessel – Schoten was built during 1844 and 1875, canal Herentals – Bocholt between 1843 and 1846. Both canals carry water from the River Meuse.

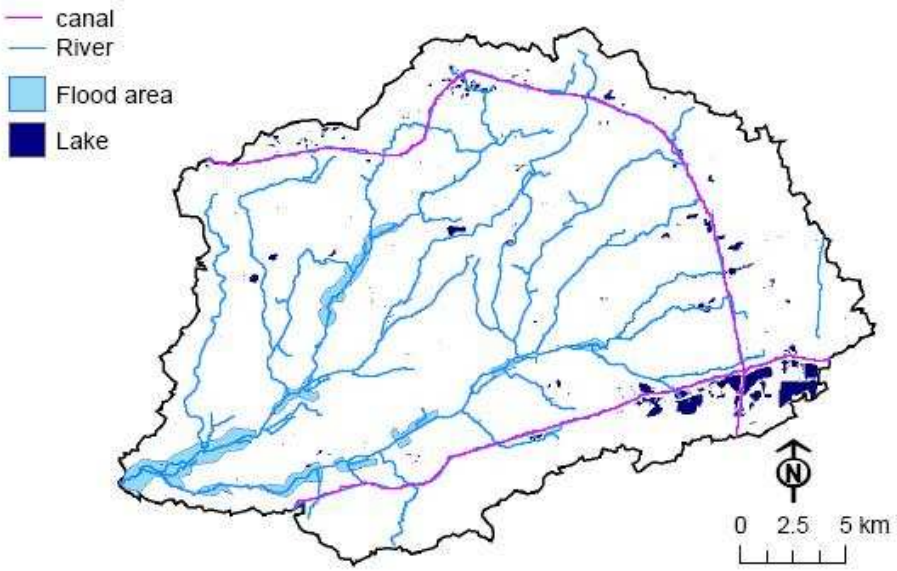

Figure 19: River, canals and lakes in the Kleine Nete basin (OC GIS Vlaanderen, 2000).

4 WetSpa

4.1 Introduction

The WetSpa model (Water and energy transfer between Soil plant and atmosphere) is a GIS-based distributed hydrological model originally developed by Wang et al. (1996) and adopted for flood prediction and water balance simulation at catchment scale by Liu and De Smedt (2004); Liu et al. (2003). The model is physically based and simulates hydrological processes of precipitation, interception, excess rainfall, soil moisture storage, interflow, percolation, evapotranspiration, groundwater storage and discharge continuously both in time and space, for which the water and energy balance is maintained on each raster cell. The simulated hydrological system consists of four control volumes: the plant canopy, the soil surface, the root zone, and the saturated groundwater aquifer (Figure 21). The model utilizes hydro-meteorological data and three basic digital maps: topography, land-use and soil type to derive the model spatial parameters with the help of ArcView scripts. The main outputs of the model are river flow hydrographs and spatially distributed hydrologic characteristics. Due to its fully distributed nature, it is a suitable model for capturing the vast amount of spatially and temporally distributed data for impact analysis studies.

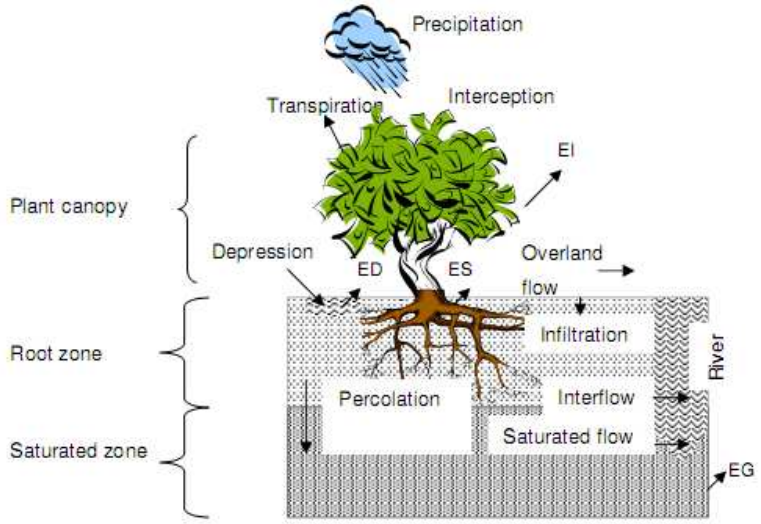

Figure 20: Hydrological processes considered in WetSpa model (Solomon, 2007).

Basic model formulation

Surface runoff for each raster cell is calculated as follows:

$$S = C_r P_n (\theta / \theta_s)$$

Equation 1

where S is the excess rainfall or surface runoff (mm), C_r is the runoff coefficient, P_n is the net precipitation, which is total precipitation less interception (mm), θ is the soil moisture content ($m^3\ m^{-3}$) and θ_s is the saturated soil moisture ($m^3\ m^{-3}$).

The surface runoff that is generated according to Equation 1 is routed from a single cell to the outlet by using the diffusive waveform of the St. Venant equation, which is given in Equation 2. This equation is used in the model to simulate both overland flow and channel flow.

$$\frac{\partial Q}{\partial t} = D\frac{\partial^2 Q}{\partial x^2} - c\frac{\partial Q}{\partial x}$$

Equation 2

where Q is the discharge (m^3 s^{-1}), x is the distance along the flow path (m), t is the time (s), c is the celerity of the wave (m s^{-1}) and D is the dissipation coefficient (m^2 s^{-1}).

Both the wave celerity c and dissipation coefficient D depend upon the flow velocity, flow depth and terrain characteristics. If the flow velocity v (m s^{-1}) is computed by Manning (Equation 3) as:

$$v = \frac{1}{n} R^{2/3} S_o^{1/2}$$

Equation 3

where R is the hydraulic radius (m), So is the slope (m m^{-1}) and n is the Manning roughness coefficient ($m^{-1/3}$ s), then the celerity of the diffusion wave c is given as:

$$c = \frac{5}{3} v$$

Equation 4

and the dispersion coefficient D is given as follows (Henderson, 1966):

$$D = \frac{vR}{2S_o}$$

Equation 5

If it is assumed that the hydraulic radius is a static terrain characteristic that does not change during a flood event, it follows from Equation 4 and Equation 5 that c and D only depend on position. In this case, an approximate solution of Equation 2 relating the discharge at the end of a flow path to the available runoff at the start is given as follows (De Smedt et al., 2000):

$$Q(t) = \frac{V}{2\sigma\sqrt{2\pi t^3 / t_o^3}} \exp\left[-\frac{(t_o - t)^2}{2\sigma^2 t / t_0}\right]$$

Equation 6

where V is the volume of surface runoff per cell (m^3) calculated as $S^*(\Delta x)^2$, with Δx the grid size (m), t_o is the total time required by the wave to travel from any point to the outlet along the topographically derived flow path and given as

$$t_o = \int \frac{dx}{c} \approx \sum_{i=1}^{n} \frac{\Delta x}{c_i}$$

Equation 7

Where n is the number of grid cells along the flow path

And σ is the deviation of the flow time

$$\sigma = \sqrt{\int \frac{2D}{c^3} dx} \approx \sqrt{\sum_{i=1}^{n} \frac{2D_i}{c_i^3} \Delta x}$$

Equation 8

Therefore, the flow routing consists of tracking the flow from a cell to the outlet along the flow path with Equation 6, and the total response is obtained by convolution of the flow response from all grid cells. The advantage of this approach is that the response functions can be obtained using standard GIS techniques. First, maps of c and D are produced using Equations 4 and 5 respectively. Next, the contributing area is determined from topographic data for a particular downstream convergence point. And for each contributing grid cells the values of t_0 and σ are calculated by using ArcInfo's FLOWLENGTH routine according to Equations 7 and 8. The interflow and groundwater contribution to the discharge are taken into account by the method of linear reservoirs (Liu and De Smedt, 2004). Finally, the total river discharge at the downstream convergence point is obtained by superimposing the surface runoff, interflow, and groundwater flow from every grid cell.

Water balance for the entire catchment is used to keep track of water changes in the hydrological system, and also as a measure of model performance by comparing the simulation results with the field observations. Among the constituents in the system, soil water content is an important state variable that influences fluxes into and out of the root zone (infiltration, evapotranspiration, percolation and interflow) and the energy balance on the land surface. Over a relatively long time period, changes in the storage of interception, depression and channel can be neglected, and the general watershed water balance can be expressed as:

$$P = RT + ET + \Delta SS + \Delta SG$$

Equation 9

where P is the total precipitation in the watershed over the simulation period (mm), RT and ET are respectively the total runoff and total evapotranspiration (mm), ΔSS is the change in soil moisture storage for the watershed between the start and the end of the simulation period (mm), and ΔSG is the change in groundwater storage of the watershed (mm).

4.2 Land-use

Land-use or land cover is an important boundary condition, which directly influence many hydrological processes. The most obvious influence of land-use on the water balance of a catchment is on the evapotranspiration process. Different land-use types have different evapotranspiration rates, due to their vegetation cover, leaf area indices, roof depths and albedo. During storms, interception and depression rates are different for different land-use types. Land-use also influences the infiltration and the soil water redistribution processes, because especially the saturated hydraulic conductivity is influenced by plant roots and pores resulting from soil fauna (Ragab & Cooper, 1993). An extreme example is the influences of build up areas and roads on overland flow. Moreover, land-use influences surface roughness, which controls overland flow velocity and floodplain flow rates. Therefore, studying the effects of future land-use configurations is one of the objectives of the present study.

The land cover classification of WetSpa model consists of fourteen classes (table 4) and it is based on the IGBP (International Geosphere-Biosphere Program) classification scheme. For each land-use type, several vegetation parameters are defined (table 5). In order to more accurately simulate the effect of vegetation on interception and evapotranspiration, a range of leaf area index and interception capacity is given in the table corresponding to the minimum and maximum values in a year for each vegetation class. Moreover, some of the parameters, such as root depth, roughness, etc., should be determined as a function of both soil type and land-use. However, for the present implementation, these parameters remain a function of the land-use only.

Tabel 4: WetSpa land-use classification.

CATEGORY	COVER
1	Crop or mixing farming
2	Short grass
3	Evergreen needle tree
4	Deciduouis needle tree
5	Deciduous broad tree
6	Evergreen broad tree
7	Tall grass
8	Irrigated crop
9	Bog marsh
10	Evergreen shrub
11	Deciduous shrub
12	Bare soil
13	Impervious area
14	Streams or open water

Tabel 5: Default parameters characterizing land-use classes.

Land-use classes	Vegetated fraction[1] (%)	Leaf area index[1] (-)	Root depth[1] (m)	Manning's coefficient[1] (-)	Interception capacity[2] (mm)
Crop or mixed farming	85	0.5 – 6.0	1.0	0.15	0.05 – 1.00
Short grass	80	0.5 – 2.0	1.0	0.20	0.05 – 1.00
Evergreen needle leaf tree	80	5.0 – 6.0	1.5	0.40	0.10 – 0.80
Deciduous needle leaf tree	80	1.0 – 6.0	1.5	0.40	0.05 – 0.80
Deciduous broad leaf tree	80	1.0 – 6.0	2.0	0.80	0.05 – 2.00
Evergreen broad leaf tree	90	5.0 – 6.0	1.5	0.60	0.15 – 2.00
Tall grass	80	0.5 – 6.0	1.0	0.40	0.10 – 1.50
Irrigated crop	80	0.5 – 6.0	1.0	0.20	0.05 – 1.00
Bog or marsh	80	0.5 – 6.0	1.0	0.20	0.05 – 1.00
Evergreen shrub	80	0.5 – 6.0	1.0	0.40	0.10 – 1.50
Deciduous shrub	80	1.0 – 6.0	1.0	0.40	0.05 – 1.50
Bare soil	5	0.5 – 2.0	1.0	0.10	0.05 – 1.00
Impervious area	0	0.0 – 0.0	0.0	0.02	0.00 – 0.00
Open water	0	0.0 – 0.0	0.0	0.02-0.05	0.00 – 0.00

[1] Rawls *et al.* (1982)
[2] Cosby et al. (1984)

The land-use maps that have been used in this study have been created by VITO (Gobin, et al., 2009) based on different GIS resources and they use a different classification scheme. To use these maps as input for the model they have been converted to the WetSpa land-use classification following the criteria in table 6.

Tabel 6: Conversion of land-use category from the original classes to the WetSpa classes.

CATEGORY	COVER (Dutch)	COVER (English)	WetSpa COVER
1	Niet beheerd grasland met biologische waarde	Grassland	short grass
2	Niet geregistreerde landbouwgrond	Grassland	short grass
3	Moeras zonder beheer	Wetland	bog mursh
4	Heide zonder beheer	Heathland	deciduous shrub
5	Kustduin zonder beheer	Coastal dunes	not present
6	Residentiële/commerciele bebouwing	Residential build up area	Impervious area (30%)
7	Agrarische bebouwing	Agricultural build up area (dispersed build up with mainly grassland)	Impervious area (40%)
8	Bedrijventerrein	Industry	Impervious area (80%)
9	Zeehaven	Port	not present
10	Luchthaven	Airport	not present
11	Grasland biodiversiteit	Grassland (natural)	short grass
12	Grasland met milieu- en natuurdoelen	Grassland (agriculture)	short grass
13	Grasland productie	Grassland (agriculture)	short grass
14	Akker met natuurdoelen	Arable land	crop or mixing farming
15	Akker met milieudoelen	Arable land	crop or mixing farming
16	Akker productie	Arable land	crop or mixing farming
17	Loofbos biodiversiteit	Forest decidious	deciduous broad leaf tree
18	Loofbos multifunctioneel	Forest decidious	deciduous broad leaf tree
19	Moeras	Wetland	bog mursh
20	Heide	Heathland	deciduous shrub
21	Kustduin	Coastal dunes	not present
22	Slik en schorre	Salt marshes	not present
23	Recreatie- en sportterreinen	recreational area	short grass
24	Parken	Park	short grass
25	Militaire voorzieningen	Militairy area	Impervious area (80%)
26	Infrastructuur	Infrastructure	Impervious area (80%)
27	Water	Water	Stream or open water
42	Naalbos biodiversiteit	Forest coniferous	Evergreen needle tree
43	Naaldbos multifunctioneel	Forest coniferous	Evergreen needle tree

4.3 Meteorology

Precipitation, potential evapotranspiration and temperature for the period 1960 until 1991 has been used as input for WetSpa model to simulate the current climate (see section 3.4.1).

4.4 Calibration

River discharge data from Grobbendonk station located at the outlet of the catchment is used for model calibration and validation. Available data ranges from Jan 1992 to Dec 2001. Model calibration was performed from the period between the 1st of January 1992 and the 31st of December 1996, while the period 1st January 1997 to 31st December 2001 was used for model verification. Figures 23 and 24 graphically compare observed and simulated daily river discharge at Grobbendonk for the years 1996 and 1998.

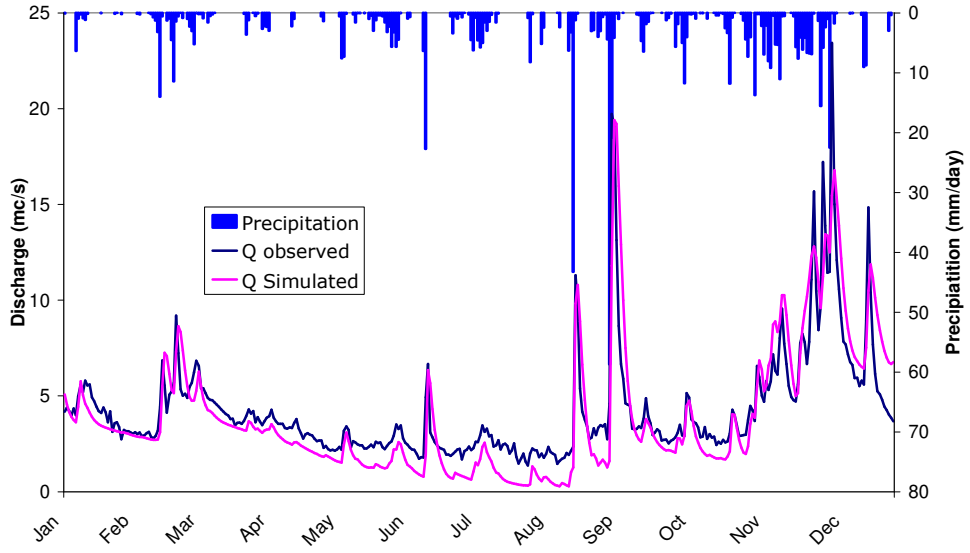

Figure 21: Graphical comparison between observed and simulated daily flow at Grobbendonk for the year 1996.

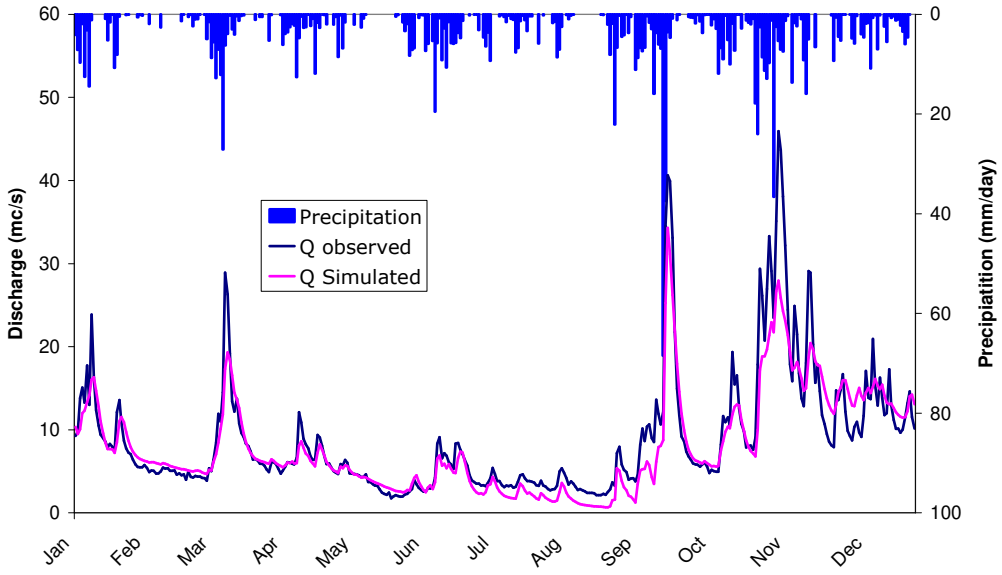

Figure 22: Graphical comparison between observed and simulated daily flow at Grobbendonk for the year 1998.

The two years represent the driest (lowest annual precipitation) and wettest (highest annual precipitation) respectively, and were chosen to show that the model performance in both cases is reasonably good.

The calibration process was done in two phases, firstly by running the model using parameters obtained from de model-independent parameter estimation model PEST (for the catchment by Banda (2005)). An attempt to derive the best possible set of global parameters using PEST was not successful due to problem of equifinality (Beven and Freer, 2001) and since PEST is sensitive to the choice of the initial guess for the parameter values. Thus, the second phase in the calibration was performed on the basis of fine-tuning the parameters by manual calibration. Manual calibration was achieved by varying a

number of parameters that include the interflow scaling factor (K_i), groundwater flow recession coefficient (K_g), initial groundwater storage (k_0), and the maximum groundwater storage (K_{max}).

In order to evaluate how well the model reproduces observed hydrographs, a series of statistical criteria given in Eqs. (10-14) are used. Table 7 shows the statistical evaluation of results for the calibration and verification periods based on criteria used by Hoffmann et al. (2004).

Tabel 7: Evaluation criteria of the model performance.

Criteria	Calibration	Validation
Model bias (C1)	-0.013	-0.132
Model determination coefficient (C2)	0.806	0.674
Nash-Sutcliffe coefficient (C3)	0.809	0.731
Model efficiency for low flows (C4)	0.675	0.617
Model efficiency for high flows (C5)	0.817	0.720

where C1, C2, C3, C4, and C5 are given by:

$$C_1 = \frac{\sum_{i=1}^{N}(Q_{Si} - Q_{Oi})}{\sum_{i=1}^{N}(Q_{Oi})}$$

Equation 10

$$C_2 = \frac{\sum_{i=1}^{N}\left(Q_{Si} - \bar{Q}_O\right)^2}{\sum_{i=1}^{N}\left(Q_{Oi} - \bar{Q}_O\right)^2}$$

Equation 11

$$C_3 = 1 - \frac{\sum_{i=1}^{N}\left(Qs_i - Qo_i\right)^2}{\sum_{i=1}^{N}\left(Qo_i - \overline{Qo}\right)^2}$$

Equation 12

$$C_4 = 1 - \frac{\sum_{i=1}^{N}\left[\ln\left(Qs_i + \varepsilon\right) - \ln\left(Qo_i + \varepsilon\right)\right]^2}{\sum_{i=1}^{N}\left[\ln\left(Qo_i + \varepsilon\right) - \overline{\ln(Q_O + \varepsilon)}\right]^2}$$

Equation 13

$$C_5 = 1 - \frac{\sum_{i=1}^{N}\left(Qo_i + \overline{Qo}\right)\left(Qs_i - Qo_i\right)^2}{\sum_{i=1}^{N}\left(Qo_i + \overline{Qo}\right)\left(Qo_i - \overline{Qo}\right)^2}$$

Equation 14

Where Qs_i is the simulated stream flow at time step I, Qo_i is the observed stream flow at time step I, N is the number of time steps in the simulated period, Qo is the mean observed stream flow for the simulated period, and ε is an arbitrary chosen small value introduced to avoid problem with nil observed or simulated stream flows. The model performs well as can be seen from graphs and statistical criteria. For both the calibration and verification period high flows are reproduced with Nash-Sutcliffe efficiency of about 75% and for low flow it is about 65%.

5 Groundwater flow modelling

5.1 MODFLOW

Numerical groundwater models employ numerical methods for solving partial differential equations that represent groundwater flow. Approximations using numerical solution techniques are attained by finite differences, finite elements, integrated finite differences, the boundary integral equation method, and analytic elements. Most models solve the general form of the 3-D groundwater flow equation, which is derived by combining Darcy's law with a water balance equation and subjected to initial and boundary conditions:

$$\frac{\partial}{\partial x}\left(K_x \frac{\partial h}{\partial x}\right)+\frac{\partial}{\partial y}\left(K_y \frac{\partial h}{\partial y}\right)+\frac{\partial}{\partial z}\left(K_z \frac{\partial h}{\partial z}\right)-W = S_s \frac{\partial h}{\partial t}$$

Equation 15

where *Kx, Ky* and *Kz* are hydraulic conductivities along the *x*-, *y*- and *z*-coordinate axes [LT^{-1}], *h* is the hydraulic head [L], *W* is a volumetric flux per unit volume that accounts for pumping, recharge, or other sources and sinks [T^{-1}], *Ss* is the specific storage [L^{-1}] and t is time [T]. The most commonly used numerical methods are the finite difference and finite element methods. Whichever method is used, the continuous region for which solution is desired must be discretized by an array of points accompanied by the generation of groundwater head equations for each nodal point (Domenico and Schwartz, 1990). The finite difference approaches utilize a regular discretization, where an aquifer is subdivided into a series of rectangular grid blocks, and describes the governing partial differential equations by methods used in differential calculus. In this study a block centred finite difference approach is applied to simulate the groundwater flow, illustrated in Fig. 23.

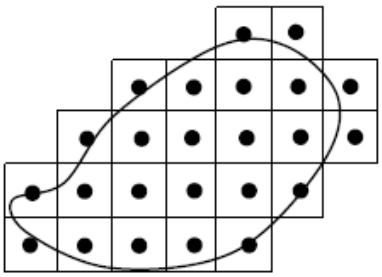

Figure 23: Discretization of an irregularly shaped aquifer with block-entered finite difference grids.

In this project the most popular industry standard code, MODFLOW (Harbaugh and McDonald, 1996) is used for simulating groundwater flow. MODFLOW is an extremely versatile finite-difference groundwater model that simulates three-dimensional groundwater flow through a porous medium. It is designed to have a modular structure that facilitates ease of understanding and ease of enhancing. MODFLOW includes procedures to simulate effects of wells, recharge, rivers, drains, evapotranspiration, and general-head boundaries, with solution algorithms that include Strongly Implicit Procedure (SIP), Slice-Successive Over Relaxation (SSOR) and Preconditioned Conjugate Gradient (PCG) iteration techniques. Layers can be either confined, unconfined or a combination of both. It is set up as a series of separate modules, which are independent; the user selects only the modules needed for the particular system that is under study.

Groundwater flow is simulated using a block centred finite difference approach. Flow regime is represented by blocks made of grids (plan view) and layers (side view). Each block is assumed to have uniform medium properties and employs eq. 15 to calculate the head for the layers by replacing the partial derivatives in the flow equation by finite differences. The heads in the top layer could rise infinitely as the model assumes unlimited vertical thickness of the top layer. When, at the end of each iteration, the head rises above the top layer elevation, the layer is considered to be confined while the opposite is true for an unconfined layer (Anderson and Woessner, 1992).

MODFLOW has been constantly updated in order to include more capabilities. The most notable recent updates are the inclusion of observation, sensitivity and parameter estimation processes that accompanied the release of MODFLOW-2000 (Hill et al., 2000).

5.2 Model description

5.2.1 Model extent and boundaries

The model consists of 722 columns and 511 rows. Pixels have a resolution of 50 meters. In total about 232400 cells are active, or about 581 km².

The horizontal boundary conditions of the groundwater model of the Kleine Nete are:

- No flow boundaries are introduced at the water divides of the Kleine Nete basin and are determined based on topographic maps, the boundary between the Kleine Nete basin and the Meuse basin in the North is taken from the Regional groundwater model of the Central Campine (Meyus, 2004).
- Rivers with known riverhead are introduces as boundary conditions inside the study area.

Vertically the groundwater flow model is limited to the quaternary and tertiary formations resting on the quasi impermeable Boom Aquitard.

5.2.2 Hydrogeological layout

The conceptual model was set up by using two layers, in order to reduce the computational burden of the model. The top layer of the model combines all the geological layers except the Miocene aquifer system, which is solely represented by the bottom layer. The horizontal hydraulic conductivity of the top layer was calculated using a weighted arithmetic mean (Domenico and Schwartz, 1990)

$$K_x = \frac{\sum m_i k_i}{\sum m_i}$$

equation 16

where K_x is the equivalent horizontal conductivity, K_i is the homogeneous conductivity of an individual layer, and m_i is the thickness of the layer. For the vertical hydraulic conductivity the weighted harmonic mean was used

$$K_z = \frac{\sum m_i}{\sum m_i / K_i}$$

equation 17

where K_z is the equivalent vertical conductivity for the layered system.

An overview of the layers used is given in Table 8.

Tabel 8: Model layers and the starting values of hydraulic conductivity used for simulation.

Model layer	Zones based on HCOV	Hydraulic conductivity	
		K_h ($m\ d^{-1}$)	K_v ($m\ d^{-1}$)
Layer 1	Zone1 (0100, 0220, 0230)	12.5 - 18.7	9.8 - 16.7
	Zone2 (0100, 0230, 0240)	1.2 – 20.0	0.1 - 18.6
	Zone3 (0100, 0230)	4.9 - 20.5	4.8 - 20.5
	Zone4 (0100, 0240)	0.1 - 4.1	0.1 - 0.6
	Zone5a (0100, 0220, 0230, 0240)	8.25 – 20.0	0.2 - 18.5
	Zone5b (0100, 0220, 0230, 0240)	10.5-19.8	0.2 - 17.8
	Zone5c (0100, 0230, 0240)	13.2 - 19.8	0.3 - 17.8
Layer 2	Zone 0250	14.1	1.4

5.2.3 River conditions

All rivers, canals and lakes are set as boundary conditions and are simulated with the river package. The simulated rivers are of category 0 (navigable), 1 and 2 (unnavigable), categorized according to the Flemish hydrological atlas. The permeability of the river sediments, the average water level, and river depth and width were determined from an inventory that was conducted for at least every 500 m for the unnavigable rivers, and at every important change in dimensions or water depth for the navigable rivers. For the calculations of the conductance of the bottom sediments, assumptions are made about the hydraulic conductivity and the thickness of the sediment bottom. Van de Moortel and Deckers (1998) determined the hydraulic conductivity of the deposits of the Scheldt. The measurements varied around 0.1 m d^{-1}. Because of the installation of leakage reducing methods on the riverbank of navigable rivers, smaller hydraulic conductivity values are assumed for the sediment bottoms of those rivers, namely 0.01 m d-1. Standard values of hydraulic conductivity and thickness of bottom sediments for all the water bodies are given in Table 9. The conductance of the river bed sediments is calculated as

$C = Kwl / d$

where C is the conductance [L^2T^{-1}], K is the permeability of the bed sediments [LT^{-1}], w is the width of the river reach [L] , l is the length of the river reach [L], d is the thickness of the bed layer [L]. The long term average water depth for unnavigable rivers was determined from observation and hydraulic models. If no data are available, standard values shown in Table 9 are used.

The flow Q [L^3/T] between aquifer and river is calculated as follows:

$Q = C (H-h)$ $\quad h > z$

With H the water level in the river [L], h the groundwater head in the aquifer [L] and z the bottom level of the river bed [L]. If the groundwater level in the aquifer sinks below the bottom level of the riverbed the flow becomes independent of the groundwater level:

$Q = C (H-z)$ $\quad h \leq z$

Tabel 9: Standard values of water depth, bottom depth, water height and width.

Surface water body	Water depth (m)	Depth to river level (m)	Depth to river bottom (m)	K (m/s)	d (m)	w (m)
River category 0	-	-	-	0.01	1	-
River category 1	1.3	1	2.3	0.1	0.5	10
River category 2	0.6	0.9	1.5	0.1	0.2	4
Canal	-	-	-	0.01	1	-
Lakes	1.5	5.5	7	0.01	2	50

The canals and lakes are mostly characterized by fixed water levels. Data for canals were provided by the authorized managers (GHA 2003a; 2003b). Data for the lakes were provided by the Flemish institution for technological investigation (VITO), and are presented in Table 10.

Tabel 10: Water level, depth and bottom slope of lakes (sand pits) operated by SCR-Sibelco.

	Water level (*m*)	Depth (*m*)	Bed elevation Slope (%)
Miramar	~ 25	10-15	16
Schans	~ 26.1	12-15	16
Maat	~ 29.7	20	16
Raaw N	~ 36.28	20	16
Raaw Z	~ 33.79	20	16
Don	~ 21.50	15-20	16

Figure 26 illustrates the model pixels for which a head dependent flux boundary is defined by the RIVER package. Rivers of category one, rivers of category 2 and the lakes and canels are shown in a different colour. For all of these pixels a river head, the hydraulic conductance of the riverbed and the elevation of the bottom of the riverbed is specified.

Rivers of category 1 incorporate the Aa River in the north and the Kleine Nete River. The head of these category 1 rivers is varied per MODFLOW stress period. Because every stress period has a length of half a month (14, 15 or 16 days) the measured river head in Grobbendonk is averaged for these half monthly periods. The river head in Grobbendonk is measured by HIC. The Vlaamse Milieu Maatschapij (VMM) has a hydraulic model of these category 1 rivers. From Joost Dewelde (VMM) we obtained a shapefile of the category 1 rivers with for each river head (discretized at 10 cm) in Grobbendonk upstream river head values. From the measured daily river head in Grobbendonk (averaged over two weeks) we created a transient river head file for the MODFLOW model for the calibration period (1996-2001).

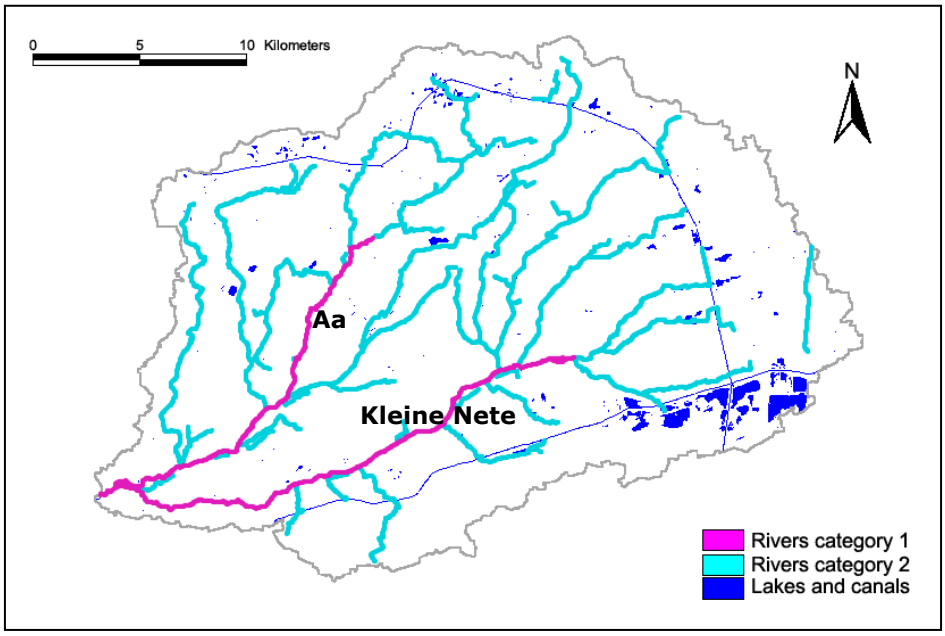

Figure 24: Head dependent flux boundaries incorporated into the model (RIVER-package).

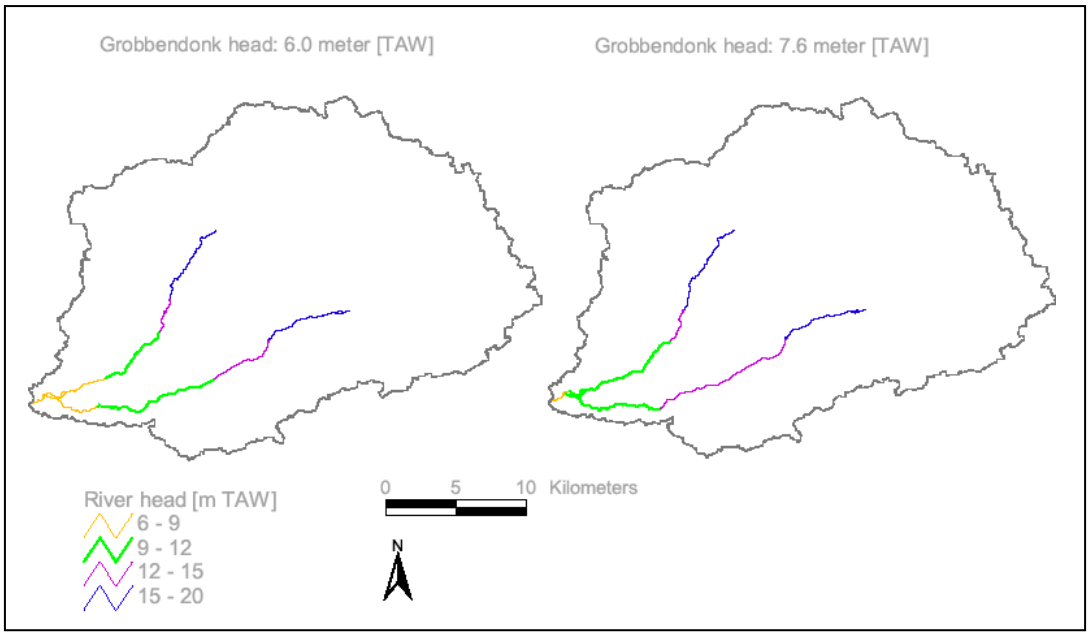

Figure 25: Transient River heads category 1 rivers.

5.2.4 Drain conditions

The drainage from unnavigable rivers of category 3 and higher and of valleys is simulated by the DRAIN-module (Harbaugh and McDonald, 1996). In this module the flow to a drain is calculated depending on the drainage level and conductance

$D = C (h - hD)$ for $h > hD$

$D = 0$ for $h \leq hD$

Where, C is the conductance [L^2T^{-1}], h is the simulated groundwater head [L] and hD is the drainage level [L].

The drainage level is set equal to the depth of the highest location in the soil profiles where rust appears. This is assumed to be the highest level groundwater will reach before it is discharged. Table 11 gives the estimated drainage levels based on the soil types of Flanders (Baeyens 1973a; 1973b). An average conductance of 40 m^2/day was used for the drains as obtained from the supra-regional model of Batelaan et al. (2000).

Tabel 11: Depths of rust appearance and drainage levels in cm below the ground level (gl) according to soil type and drainage class (Based on Stuurman et al., 2002).

Drainage class	Sand soils		Loam and clay soils	
	Rust [cm-gl]	Drainage depth [cm-gl]	Rust [cm-gl]	Drainage depth [cm-gl]
a	-	150	-	-
b	90-125	100	>125	-
c	60-90	70	80-125	80
d	40-60	40	50-80	50
h	20-40	20	30-80	20
i	0-20	10	0-30	10
e	20-40	15	30-50	15
f	0-20	5	0-30	5
g	-	0	-	0
A	>40	40	>50	50
B	>90	100	-	-
D	40-90	40	50-125	50
I	<40	10	<50	10
F	<40	5	<50	5
G	0-40	0	0-50	0

5.2.5 Well extractions

The wells are incorporated as described in section 3.5.

5.2.6 Recharge

The recharge for each stress period is calculated with the WetSpa model, described above. Recharge in the WetSpa model is calculated when infiltration minus evapotanspiration from the soil matrix exceeds the field capacity and its amount is estimated using Darcy's Law.

Because the WetSpa model has a daily timestep and the MODFLOW uses a half monthly timestep the daily recharge values calculated by WetSpa are aggregated for each MODFLOW period.

5.3 Sensitivity analysis

To determine which model parameters are important for calibration, a sensitivity analysis is carried out using the Sensitivity Processes Package of MODFLOW-2000 (Hill et al. 2000). Due to calculation time

constrains the sensitivity analysis was carried out on a steady state version of the MODFLOW model and not on the final applied transient MODFLOW model.

Dimensionless scaled sensitivities and composite scaled sensitivities are calculated as outlined in Hill (1992), Anderman et al. (1996) and Hill et al. (1998). Scaled sensitivities are given by

$$ss_{ij} = \left(\frac{\Delta h_i}{\Delta b_j} \right) b_j \omega_i^{1/2}$$

where, ss_{ij} is the scaled sensitivity; h_i is the target simulated groundwater head; b_j is the j^{th} parameter; $\Delta h_i / \Delta b_j$ is the absolute sensitivity of the simulated value with respect to the j^{th} parameter; and $\omega_i^{1/2}$ is the weight of the i^{th} observation. The term $\Delta h_i \omega_i^{1/2}$ might be dimensionless or might have the units of any of Δh_i depending on how the modeler defines $\omega_i^{1/2}$. The scaled sensitivities are used to compare the importance of different parameters in the model. When parameter estimation is considered these can be used to estimate parameters that are difficult to estimate (Hill et al. 1998). The composite scaled sensitivities indicate the total amount of information provided by the observations for the estimation of a certain parameter and are calculated as follows

$$css_j = \left[\sum_{i=1}^{\frac{1}{N}} \left(ss_{ij} \right)^2 \right]^{\frac{1}{2}}$$

where, ccs_j is the composite scaled sensitivity and N is the number of observations being used.

In order to test the sensitivity of each parameter for the hydraulic head of the model, the first layer of the model was divided into five zones as shown in Fig 26 depending on the presence/absence of geological formations as well as fault zones. The fifth zone was further divided into 3 sub zones to investigate the effect of faults that are present in the eastern part of the catchment. Wells with high pumping rates (> 1000 m^3d^{-1}) were also considered in the sensitivity analysis. The composite sensitivity of the ranked parameters and reasonable range of values for which sensitivities are tested, are presented in Table 12. The result shows that in general groundwater head levels are sensitive to recharge followed by river conductance, drain conductance and the horizontal conductivity of the geological formations. It can also be seen that piezometer head levels were least sensitive to faults, vertical hydraulic conductivity, and lake and canal conductance. Therefore, it was decided to calibrate the model only for the hydraulic conductivity of the model layers, and the conductance of the river beds, drains and lakes, while faults were not considered in the model.

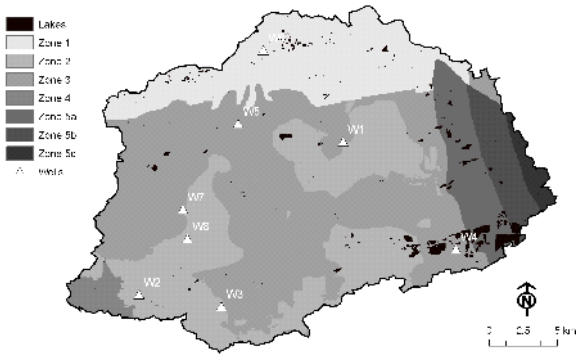

Figure 26: Zones of geological formations and wells used for sensitivity analysis

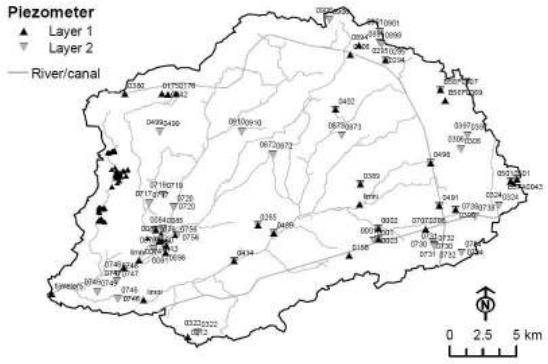

Figure 27: Piezometers used for calibration

Tabel 12: Composite sensitivity of the ranked parameters used for calibration

Rank	Parameter	Unit	Lower limit	Upper limit	Composite sensitvity (-)
1	Well 2	(%)	50	150	3.39E-02
2	Recharge zone 2	(%)	75	125	2.77E-02
3	River category 2 conductance	$m^2\ d^{-1}$	4	100	2.09E-02
4	Recharge zone 3	(%)	75	125	2.08E-02
5	Horizontal H. Conductivity zone 2 layer 2	$m\ d^{-1}$	0.1	40	1.71E-02
6	Horizontal H. Conductivity zone 6 layer 1	$m\ d^{-1}$	0.1	40	1.64E-02
7	Horizontal H. Conductivity zone 4 layer 2	$m\ d^{-1}$	0.1	40	1.34E-02
8	Recharge zone 6	(´%)	75	125	1.31E-02
9	Horizontal H. Conductivity zone 6 layer 2	$m\ d^{-1}$	0.1	40	1.20E-02
10	Recharge zone 1	(%)	75	125	1.18E-02
11	Horizontal H. Conductivity zone 1 layer 1	$m\ d^{-1}$	0.1	40	1.07E-02
12	Recharge zone 7	(%)	75	125	9.89E-03
13	Recharge zone 4	(%)	75	125	9.20E-03
14	Horizontal H. Conductivity zone 3 layer 2	$m\ d^{-1}$	0.1	40	8.99E-03
15	Horizontal H. Conductivity zone 5 layer 2	$m\ d^{-1}$	0.1	40	8.31E-03

5.4 Calibration

The transient MODFLOW model is calibrated starting from an automatic calibrated steady state version of the same MODFLOW model. Only the parameters indicated as most sensitive during the sensitivity analysis are used for the calibration. Several investigated parameter combinations are indicated in Table 13. Corresponding evaluation results are shown in Table 14.

Tabel 13: MODFLOW calibration trials of the transient model

MODFLOW parameter: Trail number	dynamic River1	Conductance River2	Horizontal hydraulic conductivity zone 2 layer 2	Horizontal hydraulic conductivity zone 6 layer 1	Horizontal hydraulic conductivity zone 4 layer 2	Horizontal hydraulic conductivity zone 6 layer 2	Horizontal hydraulic conductivity zone 1 layer 1	Horizontal hydraulic conductivity zone 3 layer 2	Drain conductance	Conductance River2
1	no	1.5	9.1	0.4	6.1	5.1	1	6.1	0.25	0.3
2	yes	1.5	9.1	0.4	6.1	5.1	1	6.1	0.25	0.3
3	yes	2	9.1	0.4	6.1	5.1	1	6.1	0.25	0.3
4	yes	10	9.1	0.4	6.1	5.1	1	6.1	0.25	0.3
5	yes	1.5	15	0.4	6.1	5.1	1	6.1	0.25	0.3
6	yes	1.5	9.1	2	6.1	5.1	1	6.1	0.25	0.3
7	yes	1.5	9.1	0.4	15	5.1	1	6.1	0.25	0.3
8	yes	1.5	9.1	0.4	6.1	10	1	6.1	0.25	0.3
9	yes	1.5	9.1	0.4	6.1	5.1	5	6.1	0.25	0.3
10	yes	1.5	5	0.4	6.1	5.1	1	6.1	0.25	0.3
11	yes	10	5	0.4	6.1	5.1	1	6.1	0.25	0.3
12	yes	1.5	9.1	0.4	6.1	5.1	1	10	0.25	0.3
13	yes	20	5	0.4	6.1	5.1	1	6.1	0.25	0.3
14	yes	10	2	0.4	6.1	5.1	1	6.1	0.25	0.3
15	yes	10	3	0.4	6.1	5.1	1	6.1	0.25	0.3
16	yes	20	5	0.3	6.1	5.1	1	6.1	0.25	0.3
17	yes	10	5	0.4	6.1	5.1	1	6.1	0.5	0.3
18	yes	10	5	0.4	6.1	5.1	1	6.1	0.7	0.3
19	yes	10	5	0.4	6.1	5.1	1	6.1	1	0.3
20	yes	10	5	0.4	6.1	5.1	1	6.1	2	0.3
21	yes	10	5	0.4	6.1	3	1	6.1	0.5	0.3
24	yes	10	7	0.4	6.1	3	1	6.1	0.5	0.3
25	yes	10	5	0.4	6.1	3	1	6.1	0.5	2
26	yes	10	5	0.4	6.1	3	1	6.1	0.5	5
27	yes	10	5	0.4	6.1	3	1	6.1	0.5	1

Tabel 14: MODFLOW calibration evaluation results

Trial number / evaluation criteria	SUM OF SQUARED WEIGHTED RESIDUALS (heads only)	average BIAS	MAE	RMSE	Nash-Sutcliff
1	56.729	0.21	0.79	1.05	0.983
2	58.641	0.22	0.81	1.06	0.983
3	56.897	0.18	0.78	1.01	0.984
4	52.119	0.11	0.66	0.85	0.989
5	67.587	0.25	0.83	1.08	0.982
6	62.266	0.14	0.89	1.30	0.974
7	58.063	0.22	0.80	1.05	0.983
8	60.51	0.18	0.85	1.19	0.978
9	59.369	0.17	0.82	1.08	0.982
10	52.359	0.19	0.78	1.04	0.983
11	47.5	0.09	0.64	0.84	0.989
12	59.2	0.18	0.82	1.07	0.982
13	47.4	0.08	0.64	0.85	0.989
14		not converging			
15	50.8	0.07	0.65	0.87	0.988
16	47.4	0.08	0.63	0.85	0.989
17	45.5	0.01	0.62	0.82	0.990
18	44.8	-0.05	0.61	0.82	0.990
19	44.2	-0.09	0.60	0.81	0.990
20	44.6	-0.19	0.60	0.83	0.989
21	45.3	0.02	0.62	0.82	0.990
24	46.6	0.02	0.62	0.83	0.990
25	43.8	-0.03	0.59	0.81	0.990
26	43.8	-0.06	0.59	0.81	0.990
27	44.2	-0.01	0.60	0.81	0.990

6 Scenarios implementation

6.1 Climate changes

Future climate scenarios are provided by the Hydraulics Laboratory of K.U.Leuven and they are produced with the CCI-HYDR Perturbation Tool (Ntegeka and Willems, 2008). More precisely we obtained three scenarios for each future year, defined as high, mean and low based on expected hydrological impacts. This definition is not dependent on the projected rainfall alone. Rather it is based on the combined effect of the rainfall and potential evapotranspiration; in other words, the variables are combined to generate an impact, which can then be classified as high, mean and low. The high scenario projects a future with wet winters and dry summers while the low scenario projects a future with dry winters and dry summers.

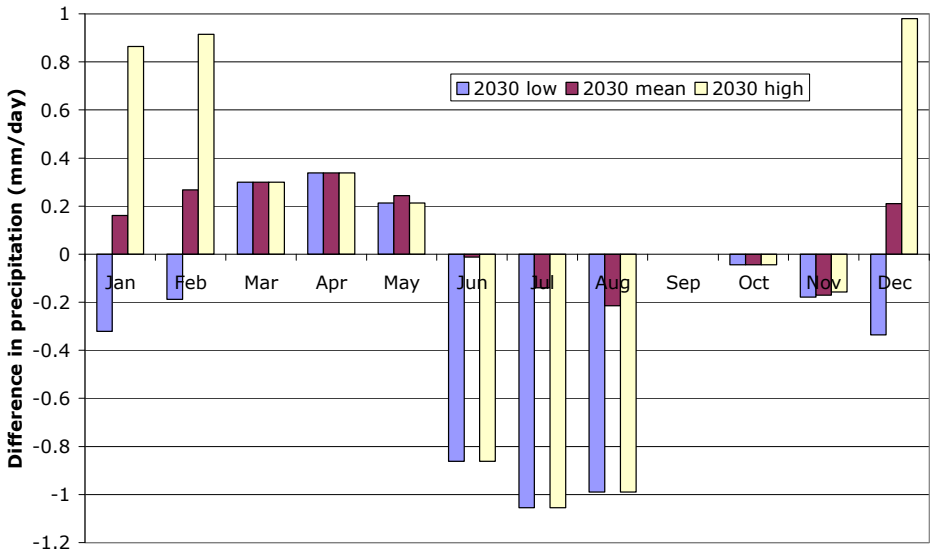

Figure 28: Monthly average for 32 years of the difference in precipitation between high, mean, low scenarios and the reference scenario.

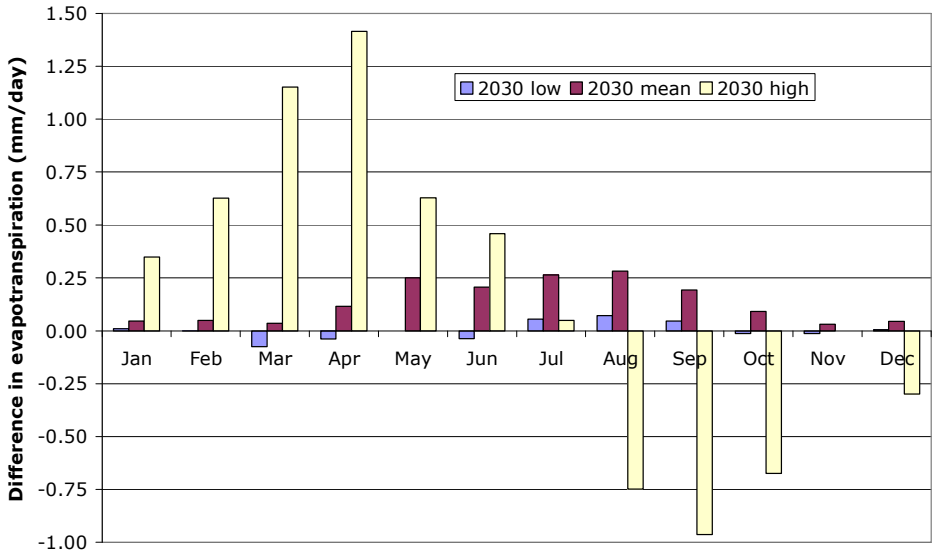

Figure 29: Monthly average for 32 years of the difference in evapotranspiration between high, mean, low scenarios and the reference scenario.

In figure 26 and 27 we show an example of comparison between these scenarios for the projection of the year 2030 regarding precipitation and evapotranspiration, respectively.

Figure 31 illustrates for a random chosen year (1981) the daily precipitation timeseries. The current timeseries is shown in dark blue, the future projections for 2030 in purple, green and light blue, respectively for the high, mean and low hydrological impact.

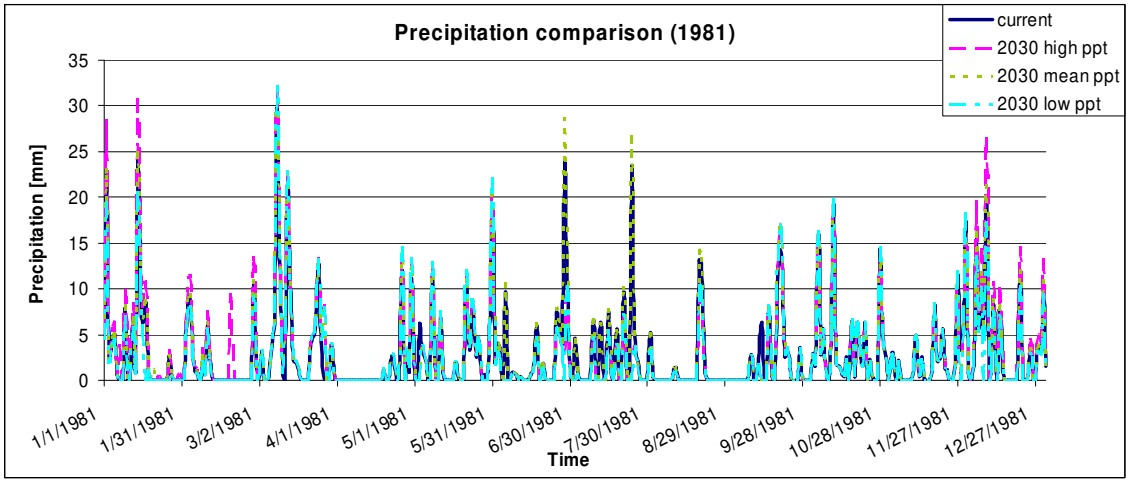

Figure 30: Daily precipitation series for the year 1981 and projected high, mean and low hydrological impact scenarios for 2030

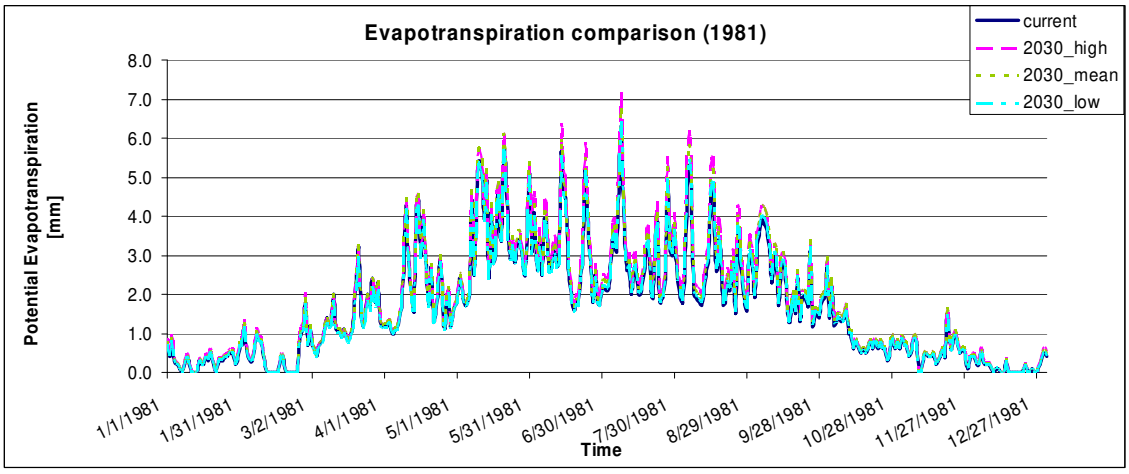

Figure 31: Daily potential evapotranspiration series for the year 1981 and projected high, mean and low hydrological impact scenarios for 2030

6.2 Land-use changes

Land-use scenarios were obtained from VITO (Gobin et al., 2009). The investigated scenarios are illustrated in Fig. 1. Figure 33 illustrates the resulting land-use maps per scenario applied in this project. The maps shown in Fig. 33 are reclassified to the land-use classes included in the WetSpa model. The small part of the basin that is located in the Netherlands is shown in white on Fig. 33, in the real model the land-use in this part of the basin is kept constant over time.

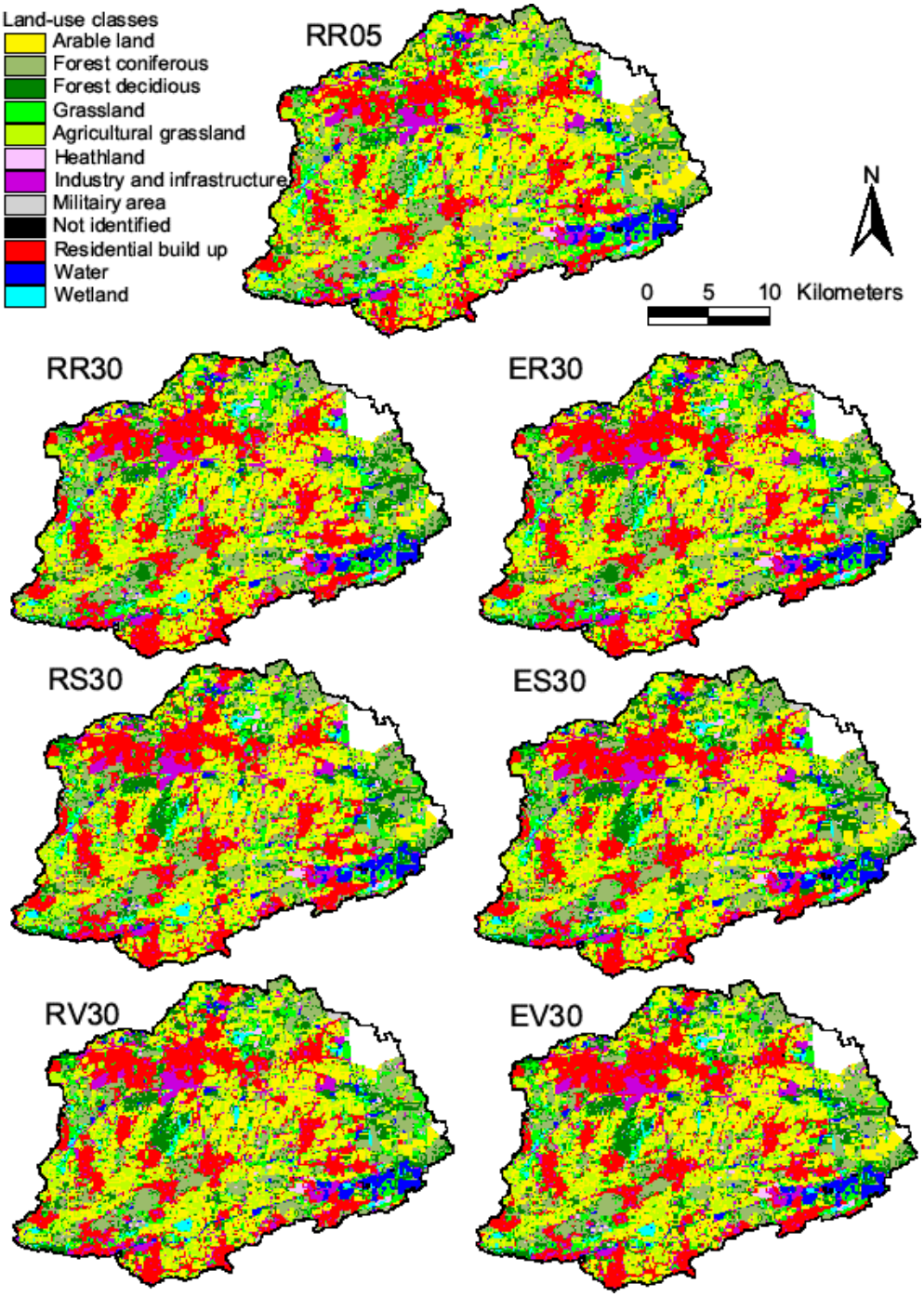

Figure 32: Current and future land-use map of the Kleine Nete basin: RR05 reference scenario 2005; RR30: reference environment and climate, reference land-use 2030; ER30: Europe environment and climate, reference land-use 2030; RS30: reference environment and climate, separate land-uses 2030; ES30: Europe environment and climate, separate land-uses 2030; RV30: Reference environment and climate, interwoven land-use 2030; EV30: Europe environment and climate, interwoven land-use 2030.

6.3 WetSpa

The scenarios, defined in section 2.3, have been implemented in the calibrated transient WetSpa model of the Kleine Nete.

Future land-use maps are provided by Toon Van Daele (INBO, 2009) and they are predictions of land cover for the year 2030. As we did for the reference scenario, these maps have been reclassified according to the conversion scheme proposed in table 6.

The maps of soil types and topography, used to simulate the future scenarios, are the same that have been used for the current condition since significant changes are not expected for the study area.

The WetSpa model simulates the groundwater recharge and the river discharge under the different scenario conditions on a daily basis, these values will be used for the implementation of the calibrated transient MODFLOW model.

6.4 MODFLOW

6.4.1 Recharge

The time variant recharge is estimated by the WetSpa model, introduced above. The daily recharge values calculated by WetSpa are aggregated for each MODFLOW stressperiod (half monthly). Before introducing the recharge into the MODFLOW model the units are converted from mm/stressperiod (WetSpa) to m/d (MODFLOW).

6.4.2 River dynamics

As explained above only the temporal dynamics of rivers of category 1 is taken into account. Rivers of category 2 along with the canals and lakes are kept constant during the entire modelling period.

Both for the current condition (1960-1991) as for the future scenarios, half monthly averaged riverhead values for Grobbendonk are not available. Therefore these riverheads are estimated based on the simulated discharge by the WetSpa model (Q). The Q–H relation was taken as

$$H = 5.5 + (0.3764 + 0.0875 * Q - 0.0007 * Q^2)$$

where H is the riverhead averaged over half a month at the Grobbendonk station [m], Q is the river discharge averaged over half a month [m^3/s] and 5.5 is the head in m TAW from the riverbed in Grobbendonk.

Similar as in the approach discussed in section 5.2.3 the estimated river head in Grobbendonk is used to select the upstream riverheads derived from the hydraulic model of the Aa and Kleine Nete Rivers (VMM).

6.4.3 Drains

The drain conditions are determined by a mixture of factors including the soil type and especially the land-use type. For the future land-use conditions the expected drain condition is estimated as follows:

Drain_new = Drain_original – AvgDrain_previousLU + AvgDrain_newLU

Where Drain_new is the new drain depth in investigated model pixel, Drain_original is the drain depth from the current condition (2005) estimated as discussed in section 5.2.3, AvgDrain_previousLU is the average drain depth for all pixels that in the current condition (2005) had the same land-use as the original land-use type of the investigated pixel, AvgDrain_newLU is the average drain depth for all pixels that in the current condition (2005) had the same land-use as the new land-use type of the investigated pixel. The average drain depths for all land-use classes during the current condition (2005) are indicated in Table 15 and Fig 35.

Tabel 15: Average drain condition (2005) per land-use type

Land-use type	Average current drain [m below soil surface]
Crop and mixing farming	0.40
Short grass	0.40
Evergreen needle tree	0.64
Deciduous needle tree	0.69
Deciduous broad tree	0.53
Tall grass	0.30
Bog or marsh	0.32
Deciduous shrub	0.45
Bare soil	1.03
Impervious area	0.78

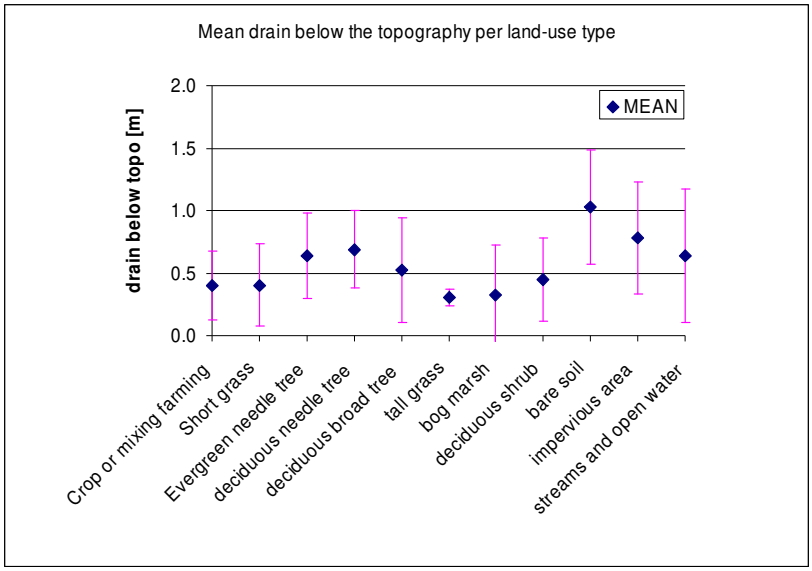

Figure 33: Graphical illustration of the mean drain per land-use type (see table 15) including the standard deviation.

7 Results

7.1 WetSpa

7.1.1 Impact of climate changes

The effect of different climate scenarios, combined with land-use scenario RR30 (table 1) on the river discharge is presented in Fig. 36. From the figure we read that the high impact scenarios of 2030 and 2100 have a similar trend; they both predict an increase in discharge in winter and spring, while in summer the discharge will decrease (slightly lower values for 2100 scenario). The same agreement can be found by observing the trends of low impact scenarios for 2030 and 2100. Moreover, for the low impact case there is less difference with the current condition.

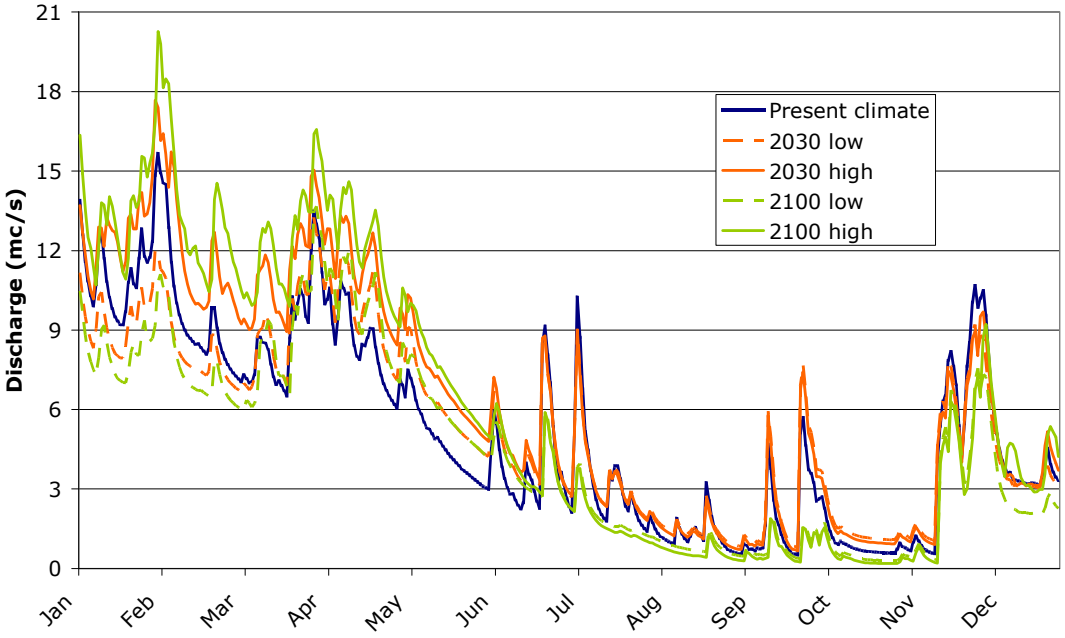

Figure 34: Comparison of the discharge predicted by the calibrated WetSpa model assuming different climate scenarios and the same land-use map (RR30).

7.1.2 Impact of land-use changes

In the following figures (37-40) we show, as example, the comparison of the discharge produced by different land-use maps and the same climate scenario (2030 high). The figures 37-40 represent the periods: January-March, April - June, July – September, October-December. The differences are very limited, just a slightly increase in the peaks of the hydrographs probably due to an increase in impervious area.

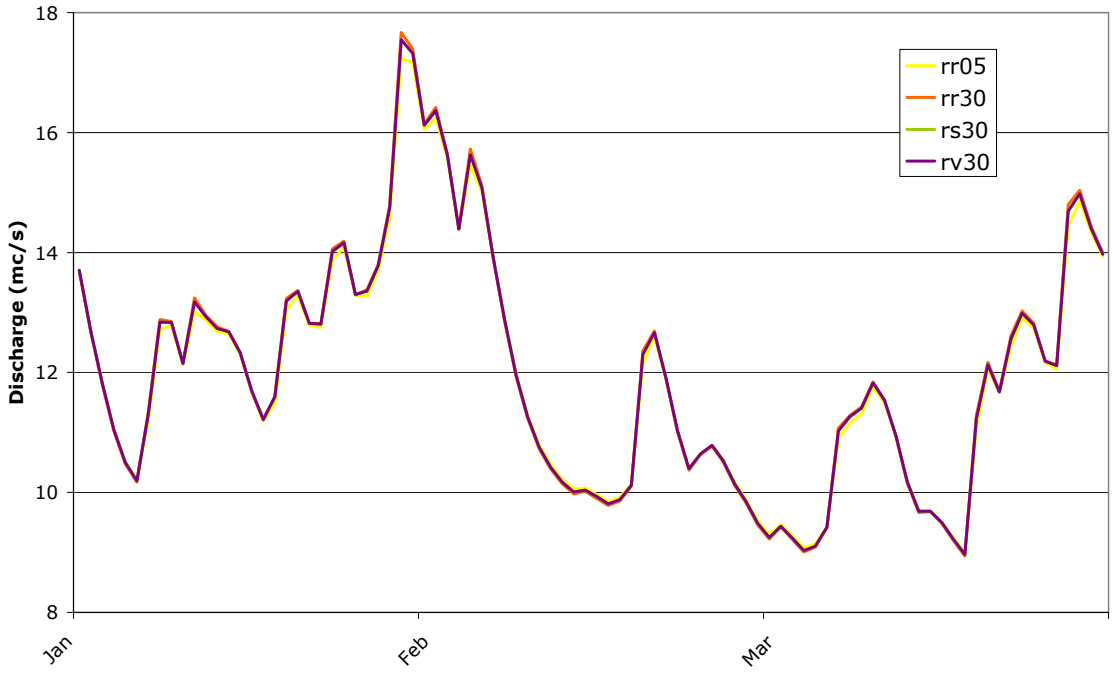

Figure 35: Comparison of the winter discharge predicted by the calibrated WetSpa model with different land-use maps and same climate scenario (2030 high).

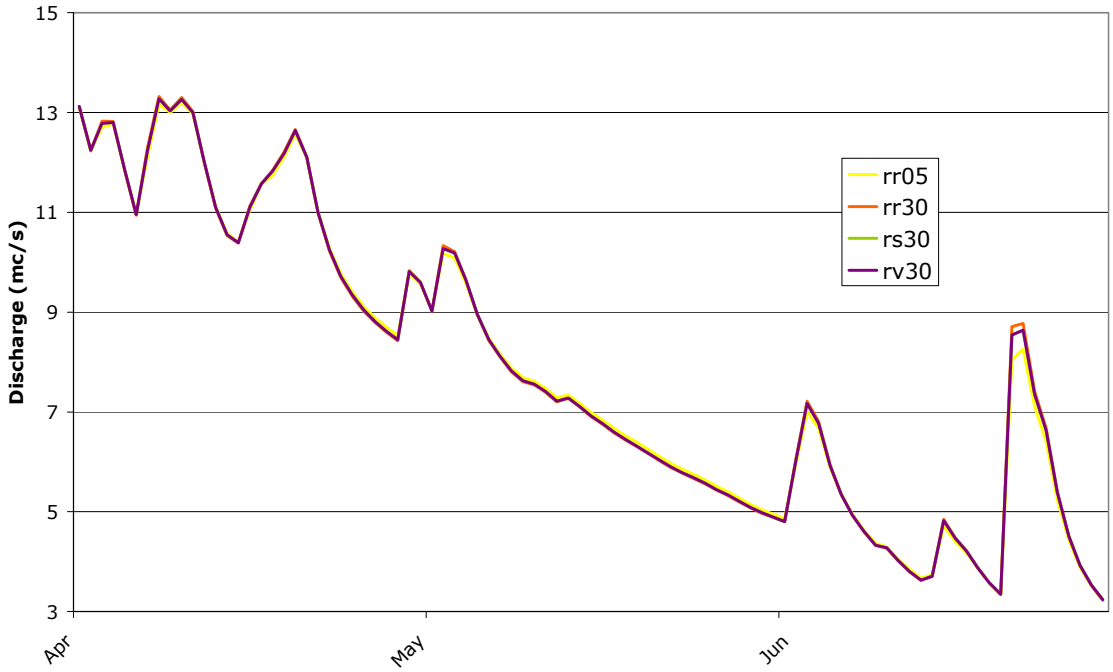

Figure 36: Comparison of the spring discharge predicted by the calibrated WetSpa model with different land-use maps and same climate scenario (2030 high).

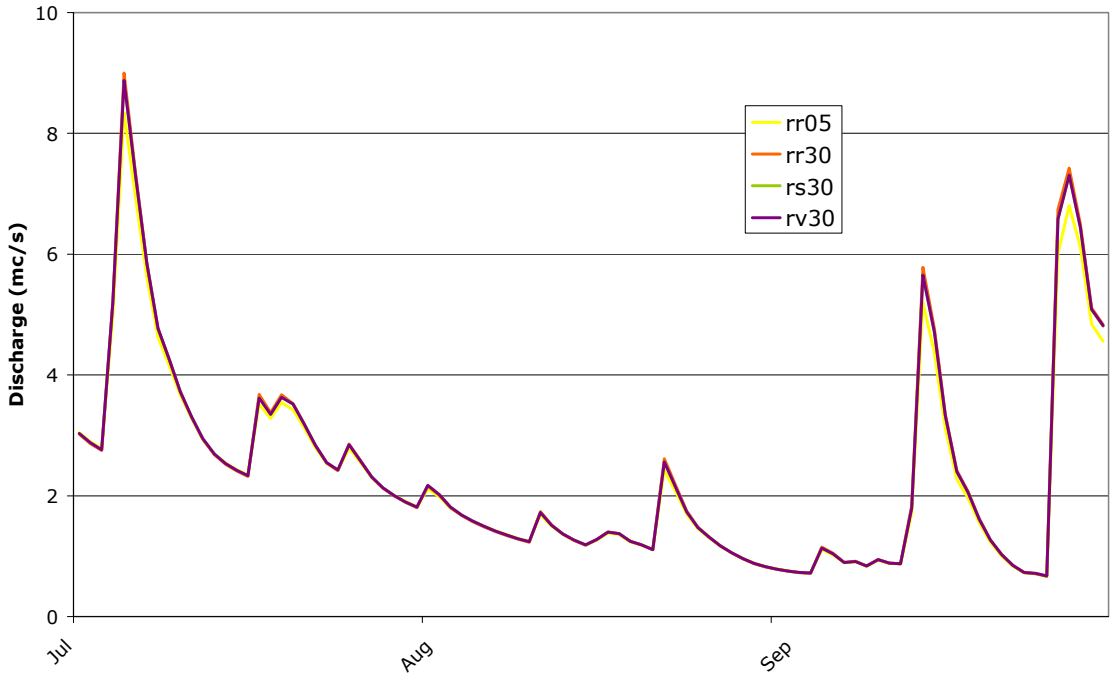

Figure 37: Comparison of the summer discharge predicted by the calibrated WetSpa model with different land-use maps and same climate scenario (2030 high).

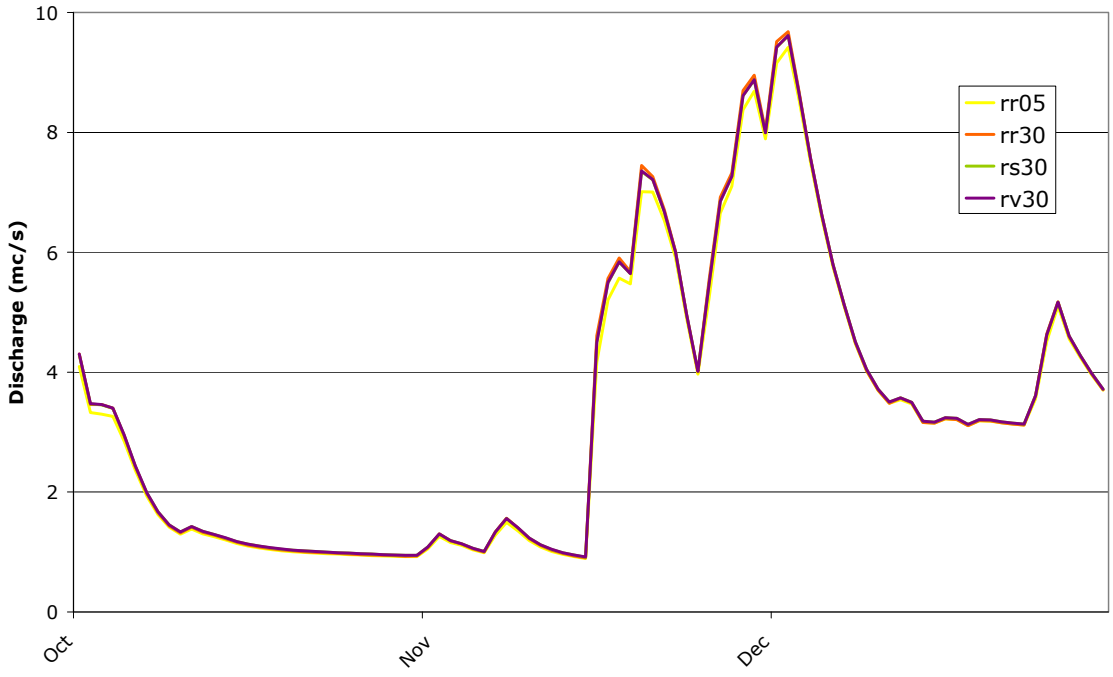

Figure 38: Comparison of the autumn discharge predicted by the calibrated WetSpa model with different land-use maps and same climate scenario (2030 high).

7.2 Groundwater model

7.2.1 Simulation of current conditions

Figure 41 illustrates some of the results of the groundwater simulations of the Kleine Nete basin, derived from modelling results applying the current climatic conditions (1960-1691) and the current (2005) land-use. The average groundwater head is shown in the left upper corner of Fig. 40. The groundwater discharge areas are clearly visible as blue areas on the figures, having a head exceeding the topography. At most places in the valley the groundwater head is between 0 and 4 meters deep. At the Campine ridge, separating the Aa en Kleine Nete valley, the groundwater table is deepest, up to 10 m. Near the upstream basin boundary the water table can also reach depths of 5 m or more.

The GXG's (average lowest/highest/spring groundwater heads) discussed in section 3.5.1 are calculated for every 50*50 meter pixel in the Kleine Nete basin based on the half monthly groundwater head results of layer 1.

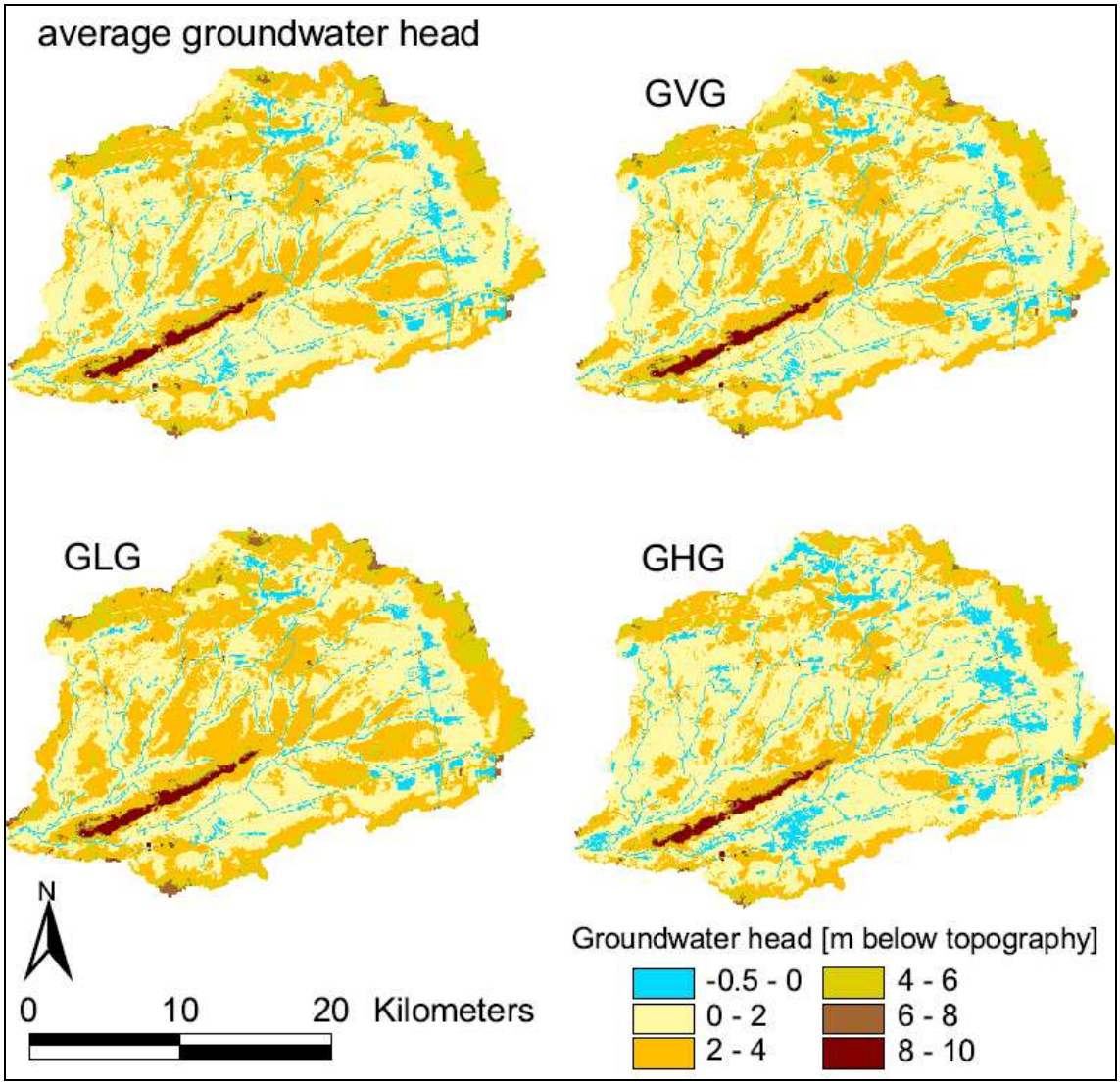

Figure 39: Average groundwater head (upper left map), average spring groundwater level (GVG) (upper right map), average lowest groundwater level (GLG) (lower left map) and average highest groundwater level (GHG) (lower right map) for the reference scenario, current climate conditions and RR05 land-use.

The upper right figure (Fig. 41) shows the average spring groundwater head (GVG). The GVG resembles very much the average groundwater head. When comparing the GHG and the GLG maps (Fig. 41) it is clear that especially on interfluves of the Aa and Kleine Nete and its tributaries and near the upstream boundaries of the Kleine Nete basin there is relatively high difference in average highest and average lowest groundwater head. Figure 42, which is the difference between the GLG and the GHG map, clearly indicates the areas where the groundwater table is more dynamic or more stable over time.

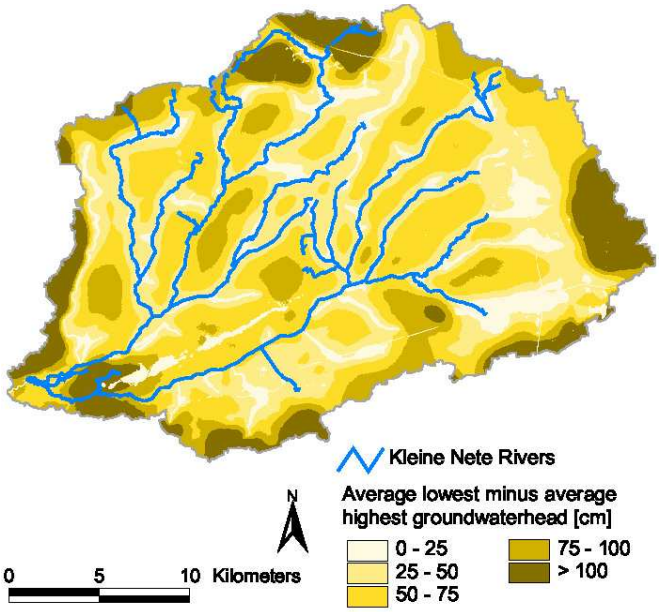

Figure 40: Average lowest groundwater head minus average highest groundwater head, reference scenario.

Figure 43 indicates the groundwater discharge areas within the Kleine Nete basin. Because both the MODFLOW drain and river package are applied in this study the map is the result of a summation of the groundwater discharge by the drain and by the groundwater flowing into the river. The resulting map shows a high to very high groundwater discharge towards the rivers with a maximum of about 550 mm/day but at most places between 50 and 200 mm/day. Groundwater discharge areas next to the river generally have a much lower discharge, at most places below 20 mm/day.

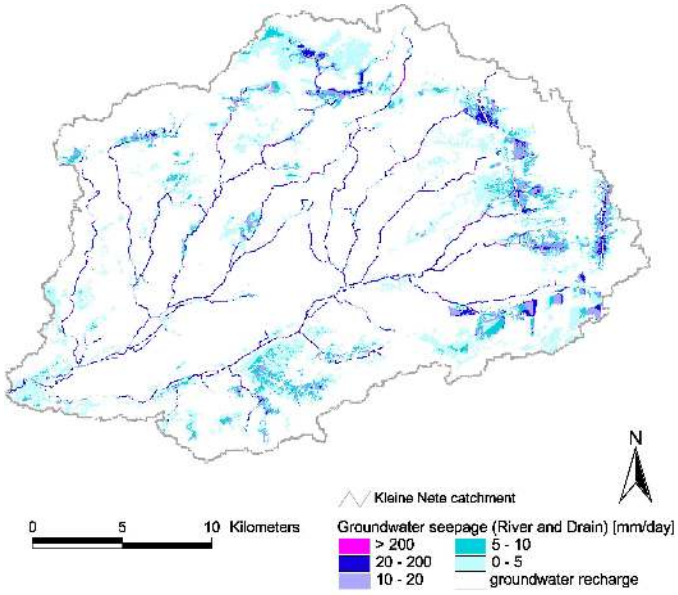

Figure 41: Simulated groundwater discharge zones in the Kleine Nete basin, reference scenario.

7.2.2 Impact of land-use changes

Figures 44 – 47 show the impact of different land-use change scenarios on the average groundwater head. In all figures the relative change with regard to the reference (2005) scenario is indicated. Blue areas indicate average groundwater head increases, yellow-brownish areas indicate average groundwater head decreases. When comparing Fig. 44, 45, 46 and 47 one can notice that in all land-use change scenarios there is a similar trend. Within the basin there are several areas where a groundwater head increase can be noticed. When comparing these areas with the current land-use (Fig 34) most of them are located near existing urban areas. In the eastern part of the catchment several pixels indicate a local decrease in average groundwater head.

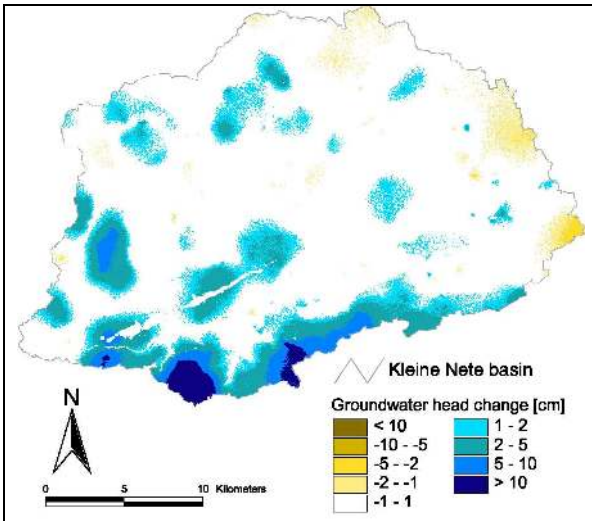

Figure 42: Average groundwater head change due to land-use change from the current land-use (2005) to the reference, reference 2030 scenario

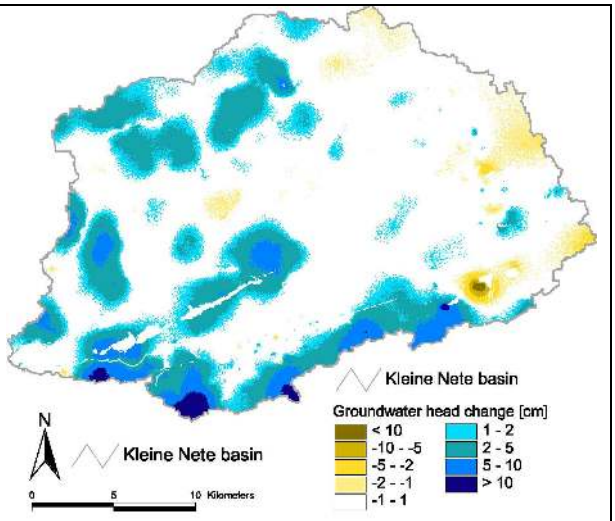

Figure 43: Average groundwater head change due to land-use change from the current land-use (2005) to the reference, land-use separation 2030 scenario

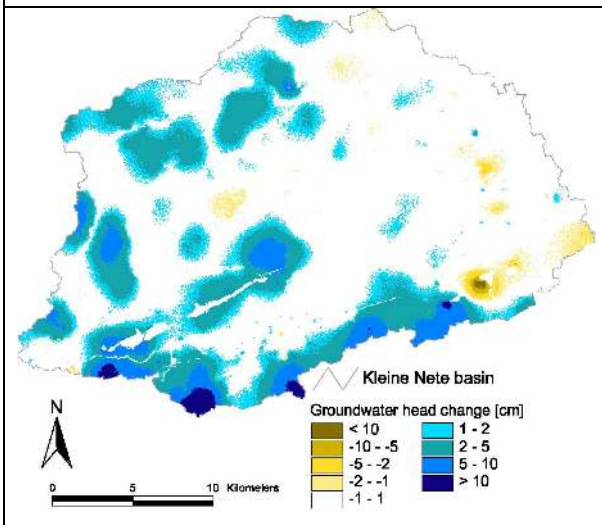

Figure 44: Average groundwater head change due to land-use change from the current land-use (2005) to the reference, land-use integration 2030 scenario

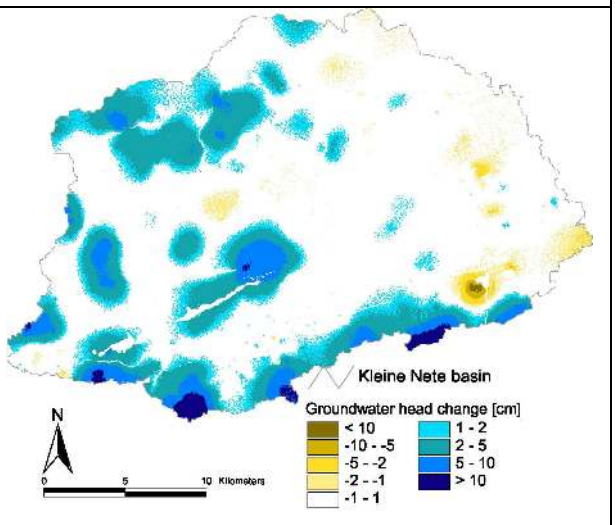

Figure 45: Average groundwater head change due to land-use change from the current land-use (2005) to the European, land-use integration 2030 scenario

Figures 48 – 51 show the impact of the same land-use changes as above on the groundwater discharge (both drain and river). The results show that the changes are relatively small, often less than 0.5 mm/day. We notice that scenarios RV30 and EV30 have more pixels with a slight decrease of groundwater discharge compared to scenarios RR30 and RS30.

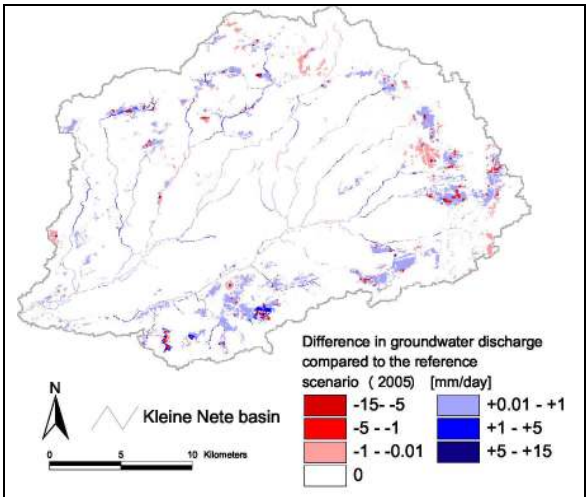

Figure 46: Comparison between the groundwater discharge of land-use change scenario RR30 with the reference scenario

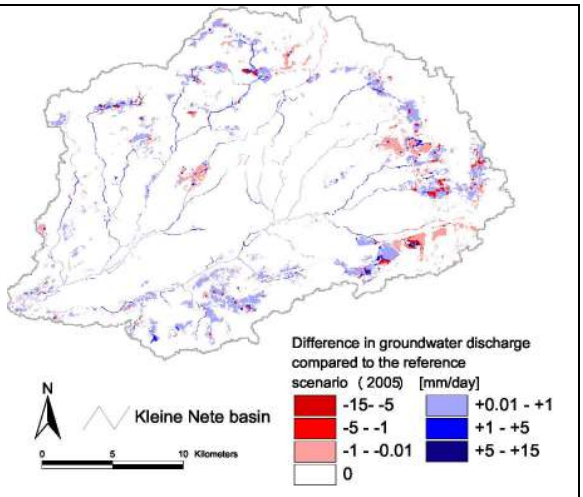

Figure 47: Comparison between the groundwater discharge of land-use change scenario RS30 with the reference scenario

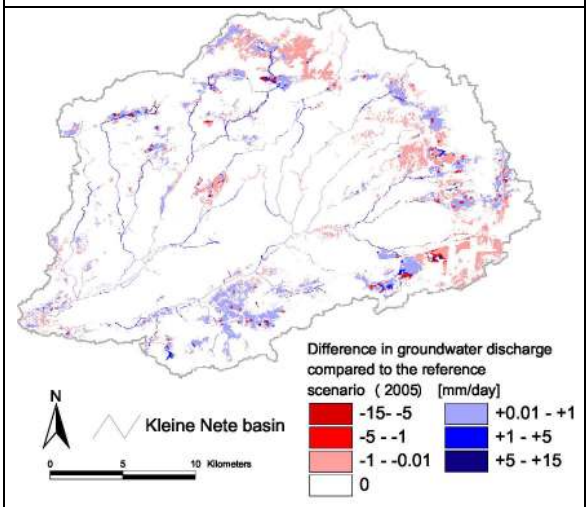

Figure 48: Comparison between the groundwater discharge of land-use change scenario RV30 with the reference scenario

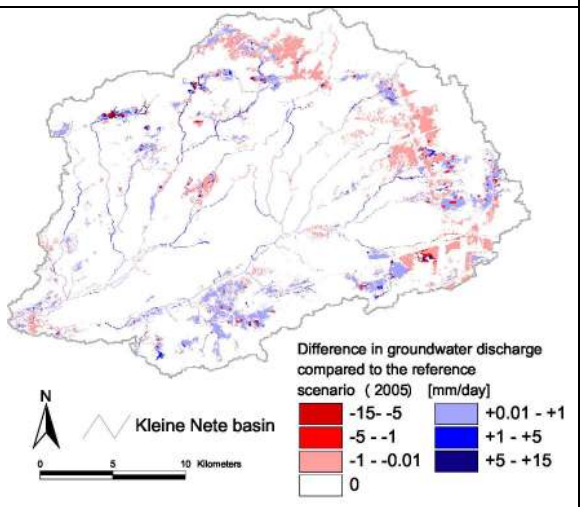

Figure 49: Comparison between the groundwater discharge of land-use change scenario EV30 with the reference scenario

Figures 52 and 53 indicate the change in average lowest and highest groundwater level due to land-use changes. The figures indicate the change in average lowest and highest groundwater level assuming land-use change scenario RR30 (Fig. 34), with the RR05 land-use as the reference point. Blue colours indicate a rise in average highest or lowest groundwater level, red colours predict a decrease with respect to the current situation. The simulated results show that both the GLG as the GHG rise at most places in the basin but rarely with more than 10 cm. On average the calculated increase of the GLG and GHG is respectively 0.85 cm and 0.78 cm.

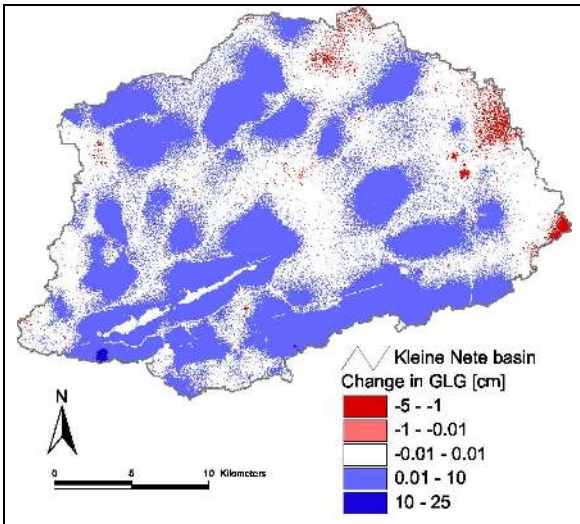

Figure 50: Change in average lowest groundwater level (GLG) due to land-use changes (RR05 to RR30).

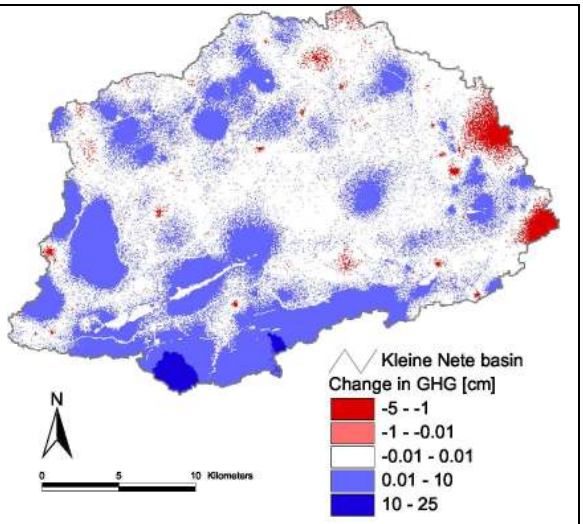

Figure 51: Change in average highest groundwater level (GHG) due to land-use changes (RR05 to RR30).

7.2.3 Impact of climate changes

The impact of the low and high impact climate change scenarios for 2100, assuming no land-use change, on the average groundwater head is shown in respectively Fig. 54 and 55. As could be expected the impact of the low impact climate change scenario on the average groundwater head is indeed much less then the impact of the high impact climate change scenario. The low impact scenario predicts a moderate decrease in roughly half the basin and a moderate increase in the other half. The high impact scenarios predict a low to high increase of the average groundwater head in almost whole the basin.

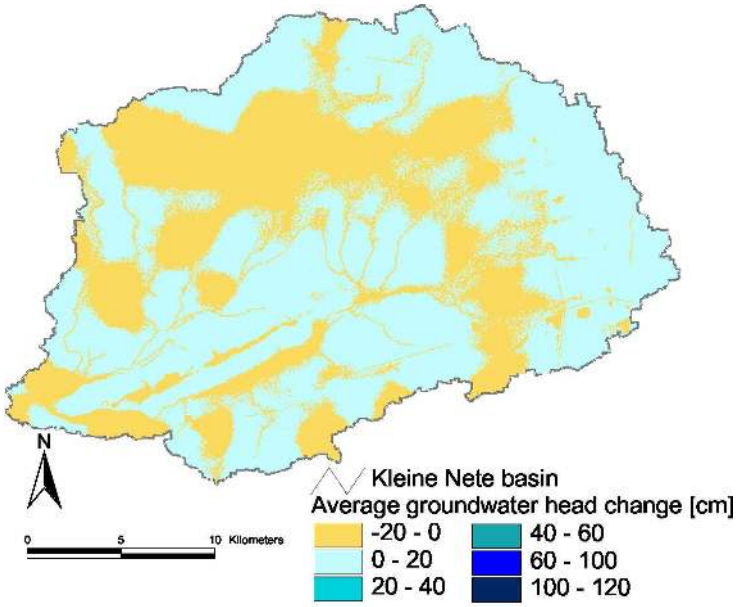

Figure 52: Average groundwater head difference between reference scenario 2005 and the scenario with no land-use change and low impact climate change 2100

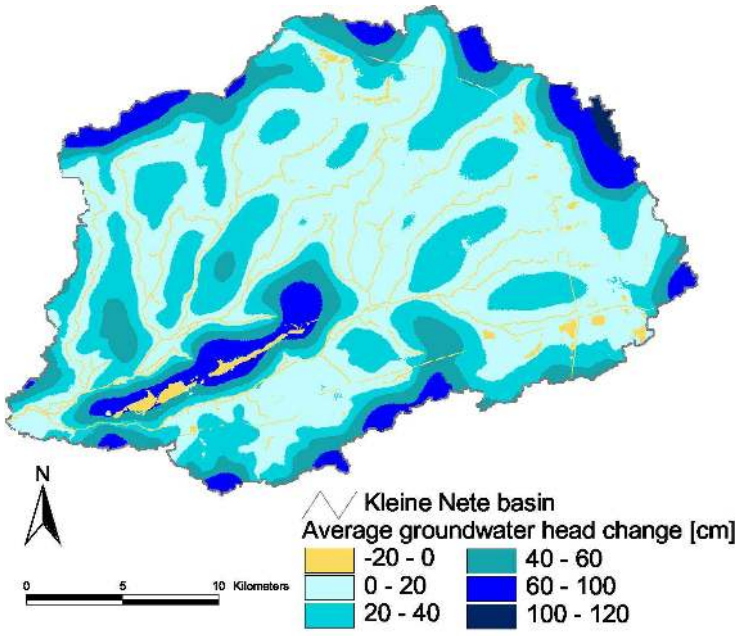

Figure 53: Average groundwater head difference between reference scenario 2005 and the scenario with no land-use change and high impact climate change 2100

Due to the importance of the groundwater dynamics for vegetation, the changes in average highest and lowest groundwater head are represented in figures 56 – 59. Figures 56 and 57 indicate the impact of respectively the GHG and GLG due to the high impact climate change scenario for 2100. Figures 58 and 59 show the impact of respectively the GHG and GLG due to the low impact climate change scenario for 2100. The high impact climate change scenario predicts a rather large increase for both the GLG and the GHG. Averaged over the entire basin the high impact scenario predicts an increase in GHG with 25.5 cm and in GLG with 15.5 cm. For the low impact climate change scenario the changes range from a decrease of the GHG and GLG, up till 17 cm and 10 cm respectively, till an increase of about 12 cm for both GHG and GLG.

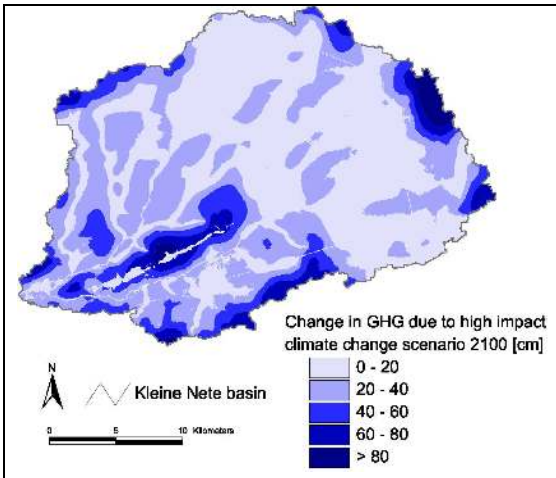

Figure 54: Change in GHG due to the high impact climate change scenario for 2100, with respect to the current condition.

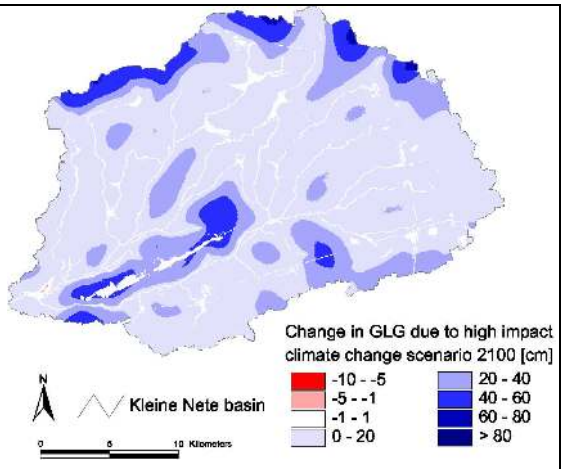

Figure 55: Change in GLG due to the high impact climate change scenario for 2100, with respect to the current condition.

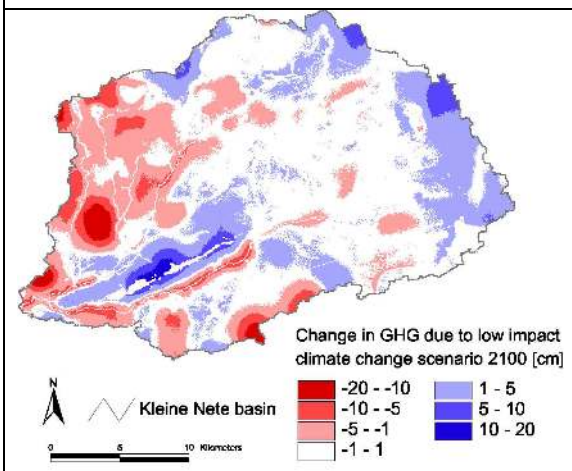

Figure 56: Change in GHG due to the low impact climate change scenario for 2100, with respect to the current condition.

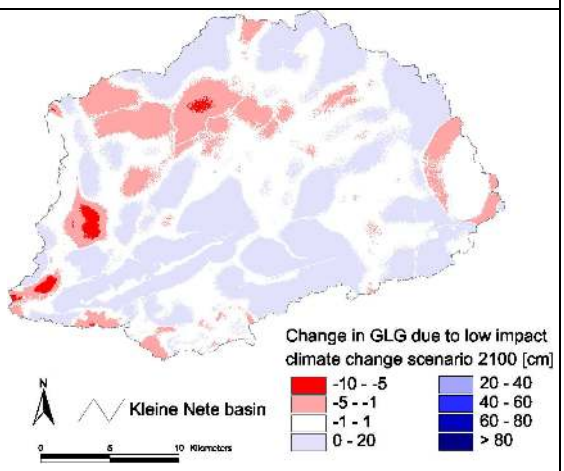

Figure 57: Change in GLG due to the low impact climate change scenario for 2100, with respect to the current condition.

7.2.4 Impact of land-use and climate changes combined

Figures 60 and 61 illustrate the combined impact of land-use and climate changes. Both scenarios assume the RR30 land-use change. Fig. 60 assumes the low impact climate change scenario for 2100, Fig. 61 assumes the high impact climate change scenario for 2100. Comparing figures 60 and 61 with the previous figures respectively 54 and 55, shows that they are very similar whether or not land-use changes occur.

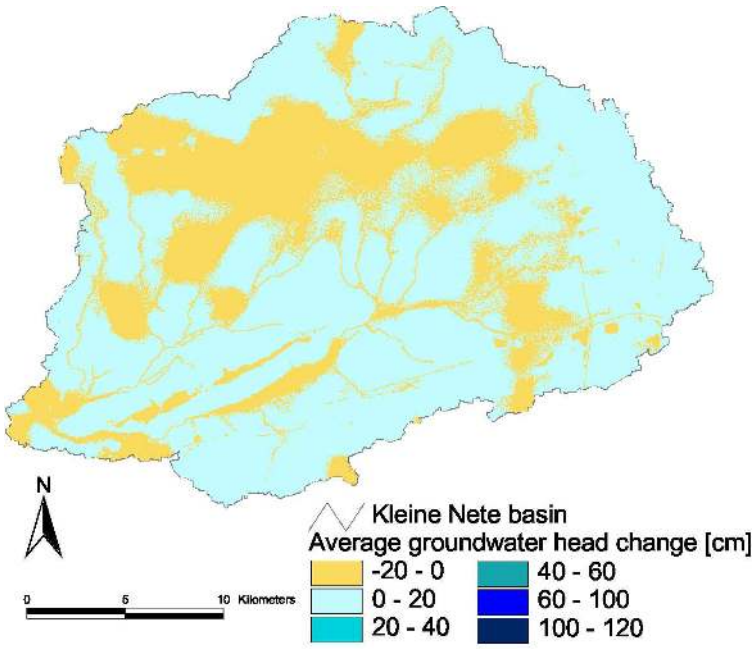

Figure 58: Average groundwater head difference between reference scenario 2005 and the scenario with land-use change RR30 and low impact climate change 2100

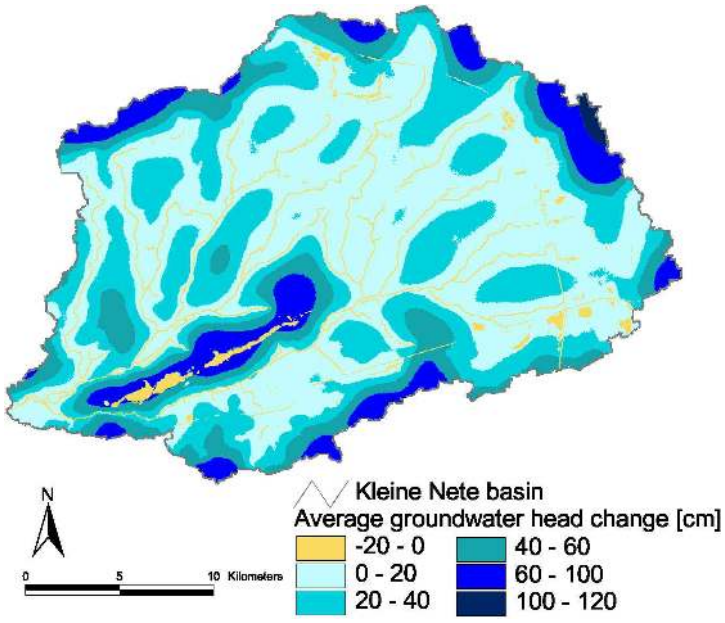

Figure 59: Average groundwater head difference between reference scenario 2005 and the scenario with land-use change RR30 and high impact climate change 2100

8 Conclusions

The impacts of human activities on water resources occur mainly through changes in land-use and climate. Those changes affect regional hydrologic balance by altering runoff, soil moisture storage, lake levels, aquifer levels, stream flow, and water quality (York et al., 2002). These alterations in turn can cause floods, draught, water supply stresses, ecological imbalance and shift in plant species. Therefore, there is a need to address these issues in order to combat possible threats posed on water resources at a catchment scale.

The aim of this project is to investigate the sensitivity and effects of future land-use and climate changes on the groundwater resources. A modelling approach that integrates available land-use and climate change scenarios into a groundwater flow model was followed in this study. This approach comprises a coupling of the hydrological model WetSpa and the groundwater flow model MODFLOW. The WetSpa model is capable of simulating the water balance components as well as spatially distributed hydrological processes at any given time step. This makes the model a powerful tool for impact assessment studies. Groundwater recharge calculations of WetSpa are integrated in the MODFLOW model along with river profiles and drain heights to study the groundwater system over time.

For the Kleine Nete catchment the WetSpa model simulates high flows satisfactorily by capturing most of the peak discharges, while low river discharges are simulated fairly well. In general, most of the river discharge consists of surface runoff and groundwater drainage, while the contribution of the interflow is much less due to the low slope angle of the catchment.

Satisfactory calibration results for the Kleine Nete MODFLOW model were achieved with respect to observed groundwater levels. The model also simulates the groundwater level fluctuations rather well. Inflow to the groundwater system mainly comes from precipitation, and a small amount from infiltration from canals, lakes and rivers. The sandy nature and shallow groundwater depth of the aquifer allows water to flow in and out of storage with relative ease, resulting in large variations in baseflow between summer and winter. This implies that changes in climatic conditions that alter the precipitation and potential evapotranspiration, can easily affect the groundwater levels, storage and drainage to the rivers.

Two climate change scenarios were fed to the Kleine Nete WetSpa model: a scenario which is expected to have a high impact and a scenario with a low expected impact on the hydrology. For the high impact scenarios WetSpa predicts a significant increase in total river discharge during winter and spring, while in summer the discharge will decrease. The same trend is observed for the low impact scenarios but with milder changes in comparison to the current condition. Also land-use changes were introduced into the WetSpa model. With regard to the total discharge, the impact of the land-use changes is low. Simulated hydrographs show that the land-use changes influences only the peak discharge, which increase slightly.

The transient groundwater flow model for the Kleine Nete simulates groundwater heads and flows for every 50 by 50 m pixel in the basin every half a month. The average groundwater head for the reference scenario shows that only at the upstream basin boundary and on the Campine ridge the groundwater depth sinks below 5 meters from the soil surface. The average spring, lowest and highest groundwater level (GVG, GLG and GHG) give an indication of the dynamic groundwater characteristics. Results show that the average groundwater depth is very similar to the GVG. The GHG minus GLG gives an indication of the dynamics of the groundwater level. Near the basin boundaries the groundwater level is more dynamic than within the basin. Near the rivers the groundwater level is most stable. The groundwater discharge map shows a high groundwater discharge into most of the major rivers (mostly between 50 and 200 mm/day). Groundwater discharge zones next to the river have a much lower discharge (mainly below 20 mm/day).

First the impact of land-use changes on the groundwater system is investigated. Comparing average groundwater head changes indicate that at many places in the basin a local increase in groundwater head is predicted. At the upstream end of the basin the average groundwater head decreases in some areas. The changes in average groundwater head are relatively similar for all investigated land-use change scenarios. Looking at the groundwater discharge zones the investigated land-use change scenarios generally result in a small change, generally lower than 1 mm/day. The land-use separation scenarios (RS30) seems to result in less zones with a groundwater discharge decrease compared to the land-use integration scenarios (RV30 and EV30), although the differences are very small. Analysing the impact of the land-use changes on the GLG and GHG, a small decrease in groundwater depth (generally less than 1 cm) is noticed in both cases assuming the RR30 future scenarios.

The impact of the climate changes on the average groundwater head is much more profound than the impact of the land-use changes. For the low impact scenario the average groundwater head changes are still relatively moderate, up to 20 cm higher or lower, for the high impact scenario the groundwater head can rise up to more than 1 meter. The high impact scenario predicts the highest increases near the basin boundaries or near the Campine ridge. Both the GLG as the GHG decrease in depth below the soil surface with the high impact climate change scenario. For the low impact climate change scenarios the changes in depth are much less and can be both up- or downwards.

For the scenarios we have analysed, the simulations show that the water balance of the catchment is more sensitive to changes in climate conditions than to land-use changes.

References

Anderson M.P., Woessner W.W., 1992. Applied groundwater modeling, simulation of flow and advective transport. Academic Press, Inc, San Diego, California, USA.

Baeyens L., 1973a. Bodemkaart van Belgë verklarende tekst bij kaartblad Kasterlee 30E. Centrum voor bodemkartering, Gent, Belgium.

Baeyens L., 1973b. Bodemkaart van Belgë verklarende tekst bij kaartblad Turnhout 17E. Centrum voor bodemkartering, Gent, Belgium.

Banda M., 2005. Estimating the effect of climate change on the hydrology of Kleine Nete catchment. MSc thesis, KUL-VUB, Belgium.

Batelaan O., Asefa T., van Campenhout A., De Smedt F., 2000. Studying the impact of land-use changes on discharge and recharge areas. In: Verhoest N.E.C., van Herpe Y.J.P., De Troch F.P. (ed) Book of abstracts of European Network of Experimental and Representative Basins (ERB) Conference. Monitoring and Modeling Catchment Water Quantity and Quality. Ghent, Belgium, 27-29 September, 2000:215-218.

Baten I. And Huybrechts, 2002. De historische bedding van de bevaarbare Nete. Verslag van het instituur voor Natuurbehoud, 2002.02, pp55.

Beven K. and Freer J., 2001. Equifinality, data assimilation, and uncertainty estimation in mechanistic modeling of complex environmental systems using the GLUE methodology. Journal of Hydrology, 249, 11-29.

De Smedt F., Liu Y.B., Gebremeskel S., 2000. Hydrological modeling on a catchment scale using GIS and remote sensed land use information, In: Brebbia C.A. (ed) Risk Analysis II, 295-304, WTI press, Southampton, Boston, USA.

Demarée G., Baguis P., Debontridder L., Deckmyn A., Pinnock S., Roulin E., Willems P., Ntegeka V. Kattenberg A., Bakker A., Bessembinder J., Lenderik G. and Beersma J., 2009. Berekining van kimaatscenarios's voor Vlaanderen. Eindverslag bij de studie met besteknummer INBO.FD.2007.5 van het Instituut voor Natuur en Bosonderzoek. Brussel, Belgium.

Domenico P.A. and Schwartz F.W., 1990. Physical and Chemical Hydrogeology. John Wiley and sons, Inc. New York, USA, pp807.

GHA (Gemeentelijk havenbedrijf Antwerpen), 2003a. Kaart met reële dokdipete.

GHA (Gemeentelijk havenbedrijf Antwerpen), 2003b. Mededelingen.

Harbaugh A.W. and McDonald M.G., 1996. User's documentation for MODFLOW-96, an update to the U.S. Geological Survey modular finite-difference ground-water flow model. US Geol. Survey Open-File report 96-485:56.

Henderson F.M., 1966. Open channel flow. Macmillan Series in Civil Engineering. New York, USA, pp522.

Hill M.C., Banta E.R., Harbaugh A.W., Anderman E.R., 200O. MODFLOW-2000, the US Geological Survey modular ground-water model – User guide to the Observation, Sensitivity, and Parameter-Estimation Processes and three post-processing programs. US Geol. Survey Open-File Report 00-184, pp210.

Hill M.C., Colley R.L. and Pollock D.W., 1998. A controlled experiment in ground-water flow model calibration using nonlinear regression. Ground Water 36, 520-535.

Hoffmann L., El Idrissi A., Pfister L., Hingray B., Guex F., Musy A., Humbert J., Drogue G., Leviandier T., 2004. Development of regionalized hydrological models in an area with short hydrological observation series. River Research and Applications 20(3), 243-254.

Liu Y.B., De Smedt F., 2004. WetSpa Extension, a GIS-based hydrological model for flood prediction and water management. Documentation and user manual. Department of Hydrology and Hydraulic Engineering, Vrije Unvierstiteit, Brussels, Belgium. [available from: www.vub.ac.be/WetSpa]

Liu Y.B., Gebremeskel S., De Smedt F., Hoffmann L. and Pfister L., 2003. A diffusive transport approach for flow routing in GIS-based flood modelling. Journal of Hydrology, 281, 91-106.

Meyus Y., Adyns D., Severyns J. Batelaan O., De Smedt F., 2004. Ontwikkeling van regionale modellen ten behoove van het Vlaams Grondwater Model (VGM) in GMS/MODFLOW. Perceel 1: Het Centraal Kempisch Model. Deelrappport 1: Basisgegevens en conceptueel model, pp131.

Ntegeka V. and Willems P., 2008. CCI-HYDR perturbation tool. A climate change tool for generating future time series for the Belgian climate. CCI-HYDR perturbation tool manual, KUL, Belgium.

OC GIS-Vlaanderen, 2001. Digital version of Land-cover data set of Flanders.

OC GIS-Vlaanderen, 2000. Digitale vectoriele bestanden van de Vlaamse Hydrografische Atlas, toestand 13/06/2000, op schaal 1/10.000, opgemaakt door MVG, LIN, AMINAL, afdeling Water (huidig: Vlaamse Milieu Maatschappij afdeling Water).

Ragab R. and Cooper J.D., 1993. Variability of unsaturated zone water transport parameters: implications for hydrological modeling. I: In situ measurements. Journal of Hydrology, 148, 109-131.

Soresma, 2002. Perceel 5 Invulling van thema's voor de uitvoering van de omgevingsanalyse in het kader van de opmaak van het bekkenbeheerplan van de Nete. Deel 2: Invulling Klimaat. In opdracht van Ministerie van de Vlaamse Gemeenschap. Dept. Leefmilieu en Infrastructuur. AMINAL, afdeling Water. Brussel.

Stuurman R., Dierckx J. And Runhaar H., 2002. Uitwerking van de methodiek voor de bepaling van de gewenste grondwatersituatie voor natuur in potentieel natte gebieden in Vlaanderen. Projectnummer 005.51027 TNO-rapport.

Van de Moortel R. And Deckers J., 1998. Bodemkundige karakterisatie van gecontroleerde overstromingsgebieden en schorren (AMIS DS8.3bis), KUL, interne publicatie nr. 49, iov AWZ afdeling Zeeschlede, pp107.

Wang Z.M., Batelaan O. and De Smedt F., 1996. A distributed model for water and energy transfer between soil, plants and atmosphere (WetSpa). Physics and Chemistry of the Earth, 21(3): 189-193.

Wemaere I., Marivoet J. and Labat S., 2008. Hydraulic conductivity variability of the Boom Clay in north-east Belgium based on four core drilled boreholes: Clays in natural and engineered barriers for radioactive waste confinement, Lille, France, 17-20 September 2007. Physics and Chemistry of the Earth, 33, p s24-s36, ISSN 1474-7065.

Woldeamlak, 2007. Spatio-temporal impacts of climate and land-use changes on the groundwater and surface water resources of a lowland catchment. Ph.D. Thesis, Vrije Universiteit Brussel, Belgium.

Wouters and Vandenberge, 1994. Geologie van de Kempen, NIRAS, Brussel.

York J.P., Person M., Gutowski W.J. and Winter T.C., 2002. Putting aquifers into atmospheric simulation models: an example from the Mill Creek Watershed, north-eastern Kansas. Advances in Water Resources, 25, 221-238.